IEEE Open Journal of Vehicular Technology

Received XX Month, XXXX; revised XX Month, XXXX; accepted XX Month, XXXX; Date of publication XX Month, XXXX.

RPDMA: A PAPR-Aware Multiple Access Scheme

GOLI SRIKANTH[1] *(Graduate Student Member, IEEE)*, SHAIK BASHEERUDDIN SHAH [2] *(Graduate Student Member, IEEE)*, NAZAR T. ALI[2] *(Senior Member, IEEE)*, VIJAY KUMAR CHAKKA [3] *(Senior Member, IEEE)*, JORGE QUEROL[1] *(Member, IEEE)*, AHMED ALTUNAIJI[2] *(Member, IEEE)*, DRAGAN OLCAN[4] *(Member, IEEE)*

[1]SnT-Interdisciplinary Center for Security, Reliability and Trust, University of Luxembourg, Luxembourg
[2]Department of Electrical Engineering, Khalifa University, Abu Dhabi, United Arab Emirates
[3]Department of Electrical Engineering, School of Engineering, Shiv Nadar University, Greater Noida, India
[4]School of Electrical Engineering, University of Belgrade, Serbia

CORRESPONDING AUTHOR: NAZAR T. ALI (e-mail: nazar.ali@ku.ac.ae).

This paper is based upon the work supported by Khalifa University under the KU-Belgrade joint research collaboration.

ABSTRACT This paper proposes a novel Multiple Access (MA) scheme called **Ramanujan Periodic-subspace Division Multiple Access (RPDMA)** for subcarrier sizes $N = 2^m,\ m \in \mathbb{N}$, to address the high Peak-to-Average Power Ratio (PAPR) in Orthogonal Frequency Division Multiple Access (OFDMA). Building on the properties of Ramanujan subspaces, we design transmitter and receiver models that allocate users on a subspace-wise basis, ensuring zero inter-user interference, providing inherent frequency diversity. We analyze the computational complexity of OFDMA, SC-FDMA, and RPDMA, and find that RPDMA has substantially lower per-user transmitter complexity than both OFDMA and SC-FDMA, while its receiver complexity is comparable to SC-FDMA and higher than that of OFDMA. We further introduce a generalized framework, termed **Nested Periodic-subspace Division Multiple Access (NPDMA)**, which unifies both RPDMA and OFDMA under a common family of multi-carrier MA schemes. We derive the theoretical PAPR of RPDMA and demonstrate its superiority over OFDMA. The analysis is validated through numerical simulations under two multi-user scenarios with diverse Quality of Service (QoS) requirements. The results demonstrate that RPDMA achieves lower PAPR than both OFDMA and SC-FDMA, with users assigned larger subspaces benefiting from even greater PAPR reduction. We prove that both the sum and per-user Spectral Efficiency (SE) of RPDMA are identical to those of OFDMA and SC-FDMA. In terms of Bit Error Rate (BER), SC-FDMA achieves the best performance, while RPDMA still outperforms OFDMA as the SNR increases.

INDEX TERMS RPDMA, Ramanujan Sum, PAPR.

I. INTRODUCTION

The emergence of demanding wireless applications, from industrial robotics and autonomous vehicles to advanced healthcare systems, requires that future 6G networks support an unprecedented diversity of Quality of Service (QoS) requirements [1], [2]. While advancing the traditional pillars of mobile broadband, massive machine-type communications, and ultra-reliable low-latency communications, 6G must also prioritize sophisticated Multiple Access (MA) schemes to meet these diverse QoS demands for critical applications [3]. This is particularly crucial for the uplink, since end-user devices such as smartphones, wearables, and IoT sensors function under stringent limitations in both power and processing capabilities [4]. Therefore, creating energy-efficient MA schemes for uplink transmission is crucial for meeting the heterogeneous QoS demands anticipated in 6G networks.

In the literature, MA schemes from 1G to 5G are broadly classified as Orthogonal Multiple Access (OMA) and Non-Orthogonal Multiple Access (NOMA) [5]. This work focuses on OMA techniques, which eliminate inter-user interference at the receiver by allocating user information orthogonally across available resources in the time, frequency, code, or space domains. The fundamental OMA techniques consist of Frequency Division Multiple Access (FDMA), Time Division Multiple Access (TDMA) [6], [7], and Code Division Multiple Access (CDMA). Subsequent evolutionary devel-

This work is licensed under a Creative Commons Attribution 4.0 License. For more information, see https://creativecommons.org/licenses/by/4.0/

opments introduced more sophisticated OMA techniques, such as: Orthogonal Frequency Division Multiple Access (OFDMA) for high Spectral Efficiency (SE) in broadband systems [8], Single Carrier FDMA (SC-FDMA) [9] for improved power efficiency in the uplink, and Spatial Division Multiple Access (SDMA) for multiplexing users in space. Modern cellular standards such as 4G Long-Term Evolution (LTE) utilize OFDMA in the downlink and SC-FDMA in the uplink [9], while 5G New Radio agreed to use only OFDMA in both the uplink and the downlink [10]. However, a well-known drawback of OFDMA is its high Peak-to-Average Power Ratio (PAPR) [11], which is especially problematic on the uplink because it forces the power amplifier to operate with a large back-off in its linear region, resulting in poor power efficiency and reduced battery life in mobile devices [12], [13]. To address the high PAPR in OFDMA, numerous reduction techniques have been proposed, which can be broadly categorized as signal pre-distortion, multiple signal candidates, coding/precoding, optimization, and Machine/Deep Learning (ML/DL). *Signal pre-distortion* methods, such as clipping, filtering, and companding, that modify the signal before transmission [11], [14]–[16], often at the cost of in-band distortion and out-of-band emission. *Multiple signal candidate* methods, including Selective Mapping (SLM) and Partial Transmit Sequence (PTS) [17]–[19], generate several candidate signals from the same data block and select the one with the lowest PAPR for transmission, trading reduced PAPR for increased computational complexity and side information. *Coding and precoding* schemes reduce PAPR by incorporating error correction or specific sequences. Examples include Golay complementary sequences [20], Fountain codes [21], Slimane's precoding [22], and Unitary precoder [23]. Some hybrid approaches that combine PTS with Gray coding are proposed in [24]. These methods can improve reliability, but may impose constraints on codebook design or require Channel State Information (CSI).

Recent studies have applied ML/DL techniques such as autoencoders [25], convolutional neural networks [26]–[28], and reinforcement learning [29] to reduce PAPR in OFDM systems. While these methods can achieve noticeable PAPR reduction through learned nonlinear signal transformations, they impose high training complexity, large memory requirements, and limited real-time adaptability. Such overheads are particularly unsuitable for uplink transmission, where user devices operate under strict power, latency, and hardware constraints. In addition, ML/DL-based approaches lack theoretical performance guarantees and face challenges in robust deployment across varying channel and system conditions [30]. Therefore, despite their potential, DL/ML-based PAPR reduction methods are beyond the scope of this work. Instead, this paper focuses on improving uplink power efficiency through transformation-based waveform design.

Beyond the above techniques, several transform-based methods have been proposed for PAPR reduction. These include the Discrete Sine/Cosine/Wavelet/Hartley Transform (DST/DCT/DWT/DHT) [31]–[34], chirp-based OFDM [35], and DCT-based Orthogonal Time Frequency and Space (OTFS) modulation [36]. While promising, these alternative schemes often require further investigation for MA scenarios [37]. Recently, the Ramanujan Periodic Transform (RPT) has gained significant attention for its applications in signal processing [38]–[46]. Employing RPT, a multi-carrier modulation scheme was introduced in [38], [47], called Ramanujan Periodic-subspace Division Multiplexing (RPDM) [48], [49]. For general non-dyadic block lengths, RPDM has been shown to achieve higher SE and lower PAPR than OFDM [48], [49], whereas for the dyadic case RPDM and OFDM have the same SE while RPDM preserves its low-PAPR property. However, extending RPDM to an MA setting remains an open challenge. In this work, we address this gap by introducing an OMA-based scheme, called Ramanujan Periodic-subspace Division Multiple Access (RPDMA), and by analyzing its PAPR characteristics in comparison with OFDMA and SC-FDMA, the primary MA techniques used in 4G/5G uplink and downlink standards [10], [50]. The key contributions of this paper are as follows:

- **RPDMA Framework:** We propose a novel multi-carrier MA scheme called RPDMA for subcarrier sizes $N = 2^m$, $m \in \mathbb{N}$. By leveraging the orthogonality of Ramanujan subspaces, we design transmitter and receiver blocks that allocate users to unique, interference-free subspaces, guaranteeing zero inter-user interference. A key advantage of this structure is its inherent frequency diversity, a feature absent in OFDMA.
- **Computational Complexity**: We analyze the computational complexity of OFDMA, SC-FDMA, and RPDMA. The analysis reveals that RPDMA achieves a substantially lower per-user transmitter complexity than both OFDMA and SC-FDMA. At the receiver, its computational cost is comparable to that of SC-FDMA and higher than that of OFDMA, which employs a single-tap equalizer. This characteristic makes RPDMA particularly attractive for uplink scenarios, where reducing the computational burden on power-limited user devices is more critical.
- **Generalization:** We introduce a broader family of multi-carrier MA schemes, called Nested Periodic-subspace Division Multiple Access (NPDMA), and show that both OFDMA and RPDMA are members of this family with zero inter-user interference.
- **PAPR Analysis:** We provide theoretical Worst-Case (WC) PAPR analysis of RPDMA for $N = 2^m$. Our results establish that RPDMA provides superior PAPR performance compared to OFDMA.
- **Numerical Simulations:** To validate the analysis, we conduct simulations under two multi-user scenarios, where users are assigned subspaces according to their QoS requirements. The results confirm RPDMA's superior PAPR performance when compared with both

OFDMA and SC-FDMA. In conventional OFDMA, PAPR increases with the number of subcarriers allocated to a user. In contrast, in RPDMA, users assigned to higher-dimensional subspaces (i.e., more subcarriers) experience lower PAPR than those assigned to lower-dimensional subspaces (i.e., fewer subcarriers).

- **SE and Bit Error Rate (BER) Analysis:** We analytically show that RPDMA attains the same SE as OFDMA and SC-FDMA. BER simulations show that, at a probability of 10^{-4}, RPDMA improves performance over OFDMA by about 2.5dB, while SC-FDMA achieves the best BER, with roughly 5dB gain over OFDMA and 2dB over RPDMA.

The remainder of this paper is organized as follows. Section II introduces the preliminaries and problem formulation. Transmitter and receiver models of RPDMA are presented in Section III, along with the NPDMA framework. Section IV provides a theoretical WC-PAPR analysis for RPDMA and OFDMA. Section V presents simulation results. Section VI presents the SE and BER analysis of RPDMA and compares it with that of OFDMA and SC-FDMA. Section VII summarizes the findings and discusses potential extensions. Finally, the paper is concluded in Section VIII.

We use the following notations throughout this paper. The sets of integers, natural numbers, real numbers, and complex numbers are denoted by $\mathbb{Z}, \mathbb{N}, \mathbb{R}$, and $\mathbb{C}$, respectively. The set of positive divisors of N is $\mathcal{D}_N = \{q_1, q_2, \ldots, q_d\}$, where $d = |\mathcal{D}_N|$ is the cardinality. For functions and operations, (k, q) represents the Greatest Common Divisor (GCD) of integers k and q, $\varphi(q)$ is Euler's totient function. Specifically, $\varphi(q)$ counts the number of integers k such that $1 \le k \le q$ and $(k, q) = 1$ [51]. We use $q \mid N$ to denote divisibility, $\mathbb{E}[\cdot]$ for expectation, and $\text{lcm}(q_1, q_2)$ for the least common multiple. We use bold lowercase letters, e.g., $\mathbf{x}$, for vectors and bold capital letters, e.g., $\mathbf{T}$, for matrices. The asymptotic upper bound on a quantity is described using $\mathcal{O}(\cdot)$. Finally, $\mathcal{CN}(0, 1)$ denotes a circularly symmetric complex Gaussian random variable with zero mean and unit variance.

II. Preliminaries and Problem Formulation

In this section, we introduce the Ramanujan Sum (RS), the Ramanujan subspace, and the RPT, and then present the problem formulation.

A. RS

For any $q \in \mathbb{N}$, the integer-valued q-periodic RS $c_q(n)$ [52] is defined as

$$c_q(n) = \sum_{\substack{k=1 \\ (k,q)=1}}^{q} e^{\frac{j2\pi kn}{q}}, \quad \forall\, n \in \mathbb{Z}, \tag{1}$$

where the summation is over all integers k from 1 to q that are coprime to q. For two distinct moduli $q_1 \neq q_2$, the sequences $c_{q_1}(n)$ and $c_{q_2}(n-\ell)$ are orthogonal over a common length-q interval, where $q = \text{lcm}(q_1, q_2)$, i.e., $\sum_{n=0}^{q-1} c_{q_1}(n)\, c_{q_2}(n-\ell) = 0, \quad \forall\, \ell \in \mathbb{Z}$.

B. Ramanujan Subspace

The $\varphi(q)$-dimensional Ramanujan subspace $\mathcal{S}_q$ is spanned by the vector $[\mathbf{c}_q]_{q\times 1} = [c_q(0), c_q(1), \ldots, c_q(q-1)]^T$ and its $\varphi(q)-1$circular downshifts [47]. Thus, any signal $x_q(n) \in \mathcal{S}_q$ is expressed as $x_q(n) = \frac{1}{\sqrt{q\varphi(q)}} \sum_{\ell=0}^{\varphi(q)-1} \gamma_\ell\, c_q(n-\ell)$, $0 \le n < q$, where γ_ℓ are expansion coefficients. Moreover, for any $N \in \mathbb{N}$, subspaces $\mathcal{S}_{q_1}$ and $\mathcal{S}_{q_2}$ are mutually orthogonal whenever $q_1 \neq q_2$ and both $q_1 \mid N$ and $q_2 \mid N$.

C. RPT

Employing the identity $\sum_{q|N} \varphi(q) = N$, the RPT decomposes an N-length signal $x(n)$ into orthogonal components associated with the divisor subspaces $\{\mathcal{S}_q\}_{q|N}$ [38], i.e.,

$$x(n) = \sum_{q|N} \underbrace{x_q(n)}_{\in \mathcal{S}_q} = \sum_{q|N} \frac{1}{\sqrt{N\varphi(q)}} \sum_{\ell=0}^{\varphi(q)-1} \gamma_{q,\ell}\, c_q(n-\ell), \tag{2}$$

where $0 \le n < N$ and $\{\gamma_{q,\ell}\}$ are the RPT coefficients. Let $\mathcal{D}_N = \{q_1, \ldots, q_d\}$ denote the set of all positive divisors of N, listed in increasing order such that $q_1 < q_2 < \cdots < q_d$. The normalization factor $\frac{1}{\sqrt{N\varphi(q)}}$ in (2) is uniquely determined by the energy of the Ramanujan subspace $\mathcal{S}_q$. For an N-length signal, the energy of the RS $c_q(n)$ over N samples is $N\varphi(q)$ [47]. This normalization ensures: (i) each basis vector has unit norm, and (ii) energy conservation. The RPT synthesis in matrix form is

$$[\mathbf{x}]_{N\times 1} = [\mathbf{T}_{\text{RPT}}]_{N\times N}\, [\mathbf{D}]_{N\times N}\, [\boldsymbol{\gamma}]_{N\times 1} = [\mathbf{T}_{\text{NRPT}}][\boldsymbol{\gamma}],$$

where $\mathbf{T}_{\text{RPT}}$ is the transformation matrix defined as

$$\mathbf{T}_{\text{RPT}} = \left[\underbrace{\mathbf{c}_{q_1}^{(0)}, \ldots, \mathbf{c}_{q_1}^{(\varphi(q_1)-1)}}_{\text{basis for } \mathcal{S}_{q_1}}, \ \ldots, \ \underbrace{\mathbf{c}_{q_d}^{(0)}, \ldots, \mathbf{c}_{q_d}^{(\varphi(q_d)-1)}}_{\text{basis for } \mathcal{S}_{q_d}} \right],$$

$\mathbf{T}_{\text{NRPT}}$ is the normalized $\mathbf{T}_{\text{RPT}}$, and $\mathbf{c}_q^{(\ell)}$ denotes the ℓ-times circular downshift of $\mathbf{c}_q$. The diagonal matrix $\mathbf{D}$ contains normalization factors. For instance, the normalization factors correspond to a subspace $\mathcal{S}_{q_k}$ are $\left[\frac{1}{\sqrt{N\varphi(q_k)}}, \ldots, \frac{1}{\sqrt{N\varphi(q_k)}}\right]_{1\times\varphi(q_k)}$ and $\boldsymbol{\gamma}$ is the RPT coefficients vector. Within each subspace $\mathcal{S}_q$, the basis vectors are mutually orthogonal *only* when $N = 2^m$ [Lemma 2 in [47]], for some $m \in \mathbb{N}$. Consequently, the RPT coefficients are computed via [Theorem 5 in [38]]

$$\boldsymbol{\gamma} = \begin{cases} \mathbf{T}_{\text{NRPT}}^T \mathbf{x} & \text{if } N = 2^m \\ \mathbf{T}_{\text{NRPT}}^{-1} \mathbf{x} & \text{if } N \neq 2^m \end{cases}. \tag{3}$$

D. Problem Formulation

Authors in [48], [49] demonstrated that RPDM, based on RPT, achieves low PAPR in single-user scenarios. However, its extension to multi-user uplink MA systems has not yet been explored. This work addresses this gap by proposing a multi-user extension of RPDM, termed RPDMA. The

objective is to develop a framework that facilitates multi-user access with diverse QoS requirements while inherently maintaining the low-PAPR characteristic, which is crucial for power-efficient uplink transmissions.

III. Multicarrier MA Uplink System

This section introduces the MA system, details the design of the RPDMA transmitter and receiver with an illustrative example, examines the frequency diversity of RPDMA, provides a comprehensive computational complexity analysis for both ends, and finally presents the NPDMA scheme.

A. MA System Model

Consider an uplink multi-carrier MA system with K users sharing $N = 2^m$ subcarriers, where $m \in \mathbb{N}$. The subcarriers are partitioned among users through disjoint sets $\{\mathcal{Q}_k\}_{k=1}^{K}$, where $\mathcal{Q}_k \subseteq \{0, 1, \ldots, N-1\}$ and $\mathcal{Q}_i \cap \mathcal{Q}_j = \emptyset$ for $i \neq j$. Let $N_k = |\mathcal{Q}_k|$ denote the number of subcarriers allocated to user k, such that $\sum_{k=1}^{K} N_k = N$. We assume ideal time and frequency synchronization at the base station receiver and neglect any hardware impairments, which is feasible in 4G/5G standards by means of timing advance and carrier frequency offset compensation mechanisms.

Each user k transmits an uncorrelated M-QAM symbol vector $\mathbf{d}_k \in \mathbb{C}^{N_k \times 1}$. Through subcarrier mapping, the k^{th} user's global frequency-domain vector $\bar{\mathbf{x}}_k \in \mathbb{C}^{N \times 1}$ is

$$\bar{\mathbf{x}}_k = \mathbf{M}_k \mathbf{d}_k \tag{4}$$

where the mapping matrix $\mathbf{M}_k \in \{0,1\}^{N \times N_k}$ is defined by

$$\mathbf{M}_k(i,j) = \begin{cases} 1 & \text{if } i = \mathcal{Q}_k(j) \\ 0 & \text{otherwise} \end{cases},$$

where $\mathbf{M}_k^T \mathbf{M}_j = \mathbf{0}$ for $k \neq j$. The time-domain transmit signal for user k is generated as

$$\mathbf{x}_k = \sqrt{\frac{P_k}{N_k}} \mathbf{E}_m \bar{\mathbf{x}}_k, \tag{5}$$

where P_k is the transmit power for user k and $\mathbf{E}_m \in \mathbb{C}^{N \times N}$ is the modulation matrix. Assuming Cyclic Prefix (CP)-based transmission over frequency-selective channels [53], the received signal at the base station after CP removal is

$$\mathbf{y} = \sum_{k=1}^{K} \mathbf{H}_{\text{cir},k} \mathbf{x}_k + \mathbf{w}. \tag{6}$$

Here $\mathbf{H}_{\text{cir},k} = \text{circ}\left([\mathbf{h}_k^T, \mathbf{0}_{1\times(N-L)}]^T\right)$ is the circulant channel matrix for user k, $\mathbf{h}_k \in \mathbb{C}^{L\times 1}$ is the channel impulse response with L-taps following i.i.d. Rayleigh fading coefficients $\sim \mathcal{CN}(0,1)$, and $\mathbf{w} \sim \mathcal{CN}(\mathbf{0}, \sigma^2\mathbf{I})$ is additive white Gaussian noise. Demodulation at the base station (receiver) yields

$$\bar{\mathbf{y}} = \mathbf{E}_d \mathbf{y} = \sum_{k=1}^{K} \sqrt{\frac{P_k}{N_k}} \underbrace{\mathbf{E}_d \mathbf{H}_{\text{cir},k} \mathbf{E}_m}_{\mathbf{H}_k} \bar{\mathbf{x}}_k + \mathbf{E}_d \mathbf{w},$$

where $\mathbf{E}_d \in \mathbb{C}^{N\times N}$ is the demodulation matrix and $\mathbf{H}_k$ is the effective channel matrix for user k. After decoupling, user k's data $\bar{\mathbf{y}}_k$ is extracted as follows:

$$\bar{\mathbf{y}}_k = \mathbf{M}_k^T \bar{\mathbf{y}} = \sqrt{\frac{P_k}{N_k}} \underbrace{\mathbf{M}_k^T \mathbf{H}_k \mathbf{M}_k}_{\mathbf{G}_k} \mathbf{d}_k + \underbrace{\mathbf{M}_k^T \mathbf{E}_d \mathbf{w}}_{\bar{\mathbf{w}}_k} + \underbrace{\sum_{j\neq k} \sqrt{\frac{P_j}{N_j}} \underbrace{\mathbf{M}_k^T \mathbf{H}_j \mathbf{M}_j}_{\mathbf{G}_{j,k}} \mathbf{d}_j}_{\text{inter-user interference}}.$$

The effective channel matrices are $\mathbf{G}_k \in \mathbb{C}^{N_k \times N_k}$ (desired signal) and $\mathbf{G}_{j,k} \in \mathbb{C}^{N_k \times N_j}$ (interference) with $\bar{\mathbf{w}}_k \sim \mathcal{CN}\left(\mathbf{0}, \sigma^2 \mathbf{M}_k^T \mathbf{E}_d \mathbf{E}_d^H \mathbf{M}_k\right)$ be the effective noise vector.

Let $S_{N,k}(n) = \frac{1}{\sqrt{N}} e^{j2\pi kn/N}, \quad 0 \leq n \leq N-1$. Then, the $N \times N$ normalized DFT matrix is

$$\mathbf{T}_{\text{NDFT}} = \left[S_{N,0}(n),\, S_{N,1}(n),\, \ldots,\, S_{N,N-1}(n)\right]. \tag{7}$$

If $\mathbf{E}_m = \mathbf{T}_{\text{NDFT}}$ and $\mathbf{E}_d = \mathbf{T}_{\text{NDFT}}^H$, then the system corresponds to conventional OFDMA. Since DFT matrices diagonalize circulant matrices, we obtain $\mathbf{G}_k = \mathbf{\Lambda}_k$ (a diagonal matrix) and $\mathbf{G}_{j,k} = \mathbf{0}$, which implies

$$\bar{\mathbf{y}}_k = \sqrt{\frac{P_k}{N_k}} \mathbf{\Lambda}_k \mathbf{d}_k + \bar{\mathbf{w}}_k. \tag{8}$$

B. RPDMA

Building on the RPT framework discussed in Section II, we propose *RPDMA* for $N = 2^m$, a novel MA scheme leveraging the orthogonal decomposition properties of RPT. Unlike conventional OFDMA that allocates arbitrary subcarriers, RPDMA assigns each user k to a distinct divisor, say q_k, of N, where $q_k \in \tilde{\mathcal{D}}_N = \{q_1, q_2, \ldots, q_d\}$ with $d = |\tilde{\mathcal{D}}_N| = m+1$. Here, indices 1 to d serve only as labels and do not imply any ordering of the elements. Consequently, user k exclusively occupies $\varphi(q_k)$ subcarriers belong to $\mathcal{S}_{q_k}$. The maximum number of supported users is $K \leq d$, with $\sum_{k=1}^{d} \varphi(q_k) = N$ ensuring complete basis utilization.

1) Transmitter and Receiver Design

Each user k transmits an M-QAM symbol vector $\mathbf{d}_k \in \mathbb{C}^{\varphi(q_k)\times 1}$. The global QAM vector $\bar{\mathbf{x}}_k \in \mathbb{C}^{N\times 1}$ is constructed through subspace mapping as $\bar{\mathbf{x}}_k = \mathbf{M}_k \mathbf{d}_k$, where $\mathbf{M}_k \in \{0,1\}^{N\times\varphi(q_k)}$ maps $\mathbf{d}_k$ to the indices of subcarriers belong to $\mathcal{S}_{q_k}$. The time-domain signal is synthesized using the normalized modulation matrix $\mathbf{T}_{\text{NRPT}}$:

$$\mathbf{x}_k = \sqrt{\frac{P_k}{\varphi(q_k)}} \mathbf{T}_{\text{NRPT}} \bar{\mathbf{x}}_k. \tag{9}$$

After inserting the CP, $\mathbf{x}_k$ is transmitted over the frequency-selective channel. At the base station, the received signal, following CP removal and subsequent demodulation, is

$$\bar{\mathbf{y}} = \sum_{k=1}^{K} \sqrt{\frac{P_k}{\varphi(q_k)}} \mathbf{T}_{\text{NRPT}}^T \mathbf{H}_{\text{cir},k} \mathbf{T}_{\text{NRPT}} \bar{\mathbf{x}}_k + \mathbf{T}_{\text{NRPT}}^T \mathbf{w}. \tag{10}$$

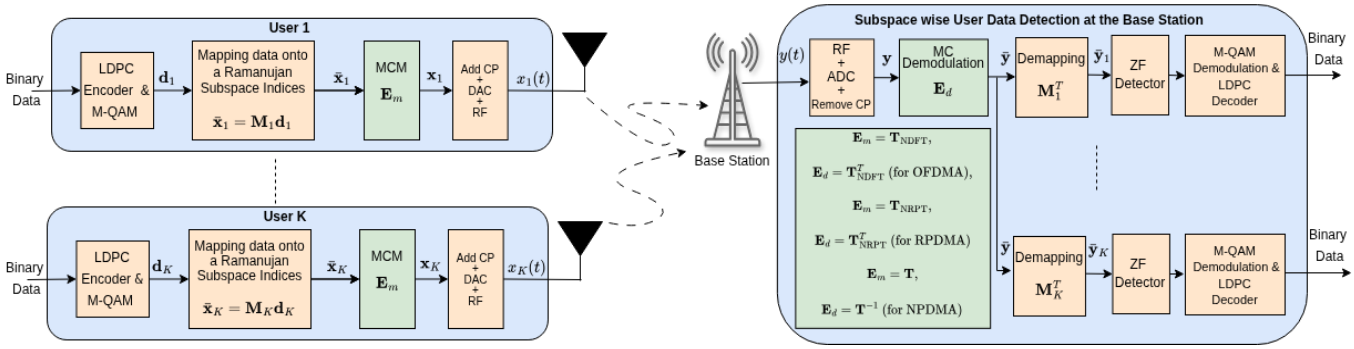

FIGURE 1. **Block diagram of a typical transform-domain uplink MA scheme. By selecting $\mathbf{E}_m$ and $\mathbf{E}_d$ appropriately, the same architecture realizes OFDMA ($\mathbf{E}_m = \mathbf{T}_{\text{NDFT}}$, $\mathbf{E}_d = \mathbf{T}_{\text{NDFT}}^H$), RPDMA ($\mathbf{E}_m = \mathbf{T}_{\text{NRPT}}$, $\mathbf{E}_d = \mathbf{T}_{\text{NRPT}}^T$), or, more generally, an NPDMA scheme with an arbitrary NPM $\mathbf{T}$.**

User k's signal is extracted via the demapping matrix as

$$\bar{\mathbf{y}}_k = \mathbf{M}_k^T\bar{\mathbf{y}} = \sqrt{\frac{P_k}{\varphi(q_k)}}\mathbf{G}_k\mathbf{d}_k + \sum_{j\neq k}\sqrt{\frac{P_j}{\varphi(q_j)}}\mathbf{G}_{j,k}\mathbf{d}_j + \bar{\mathbf{w}}_k, \tag{11}$$

where the desired and interference channel matrices are

$$[\mathbf{G}_k]_{\varphi(q_k)\times\varphi(q_k)} = \mathbf{M}_k^T\mathbf{T}_{\text{NRPT}}^T\mathbf{H}_{\text{cir},k}\mathbf{T}_{\text{NRPT}}\mathbf{M}_k, \tag{12}$$

$$[\mathbf{G}_{j,k}]_{\varphi(q_k)\times\varphi(q_j)} = \mathbf{M}_k^T\mathbf{T}_{\text{NRPT}}^T\mathbf{H}_{\text{cir},j}\mathbf{T}_{\text{NRPT}}\mathbf{M}_j. \tag{13}$$

From Proposition I in [48], the circulant channel is block diagonalized in the RPT domain:

$$\mathbf{T}_{\text{NRPT}}^T\mathbf{H}_{\text{cir},k}\mathbf{T}_{\text{NRPT}} = \begin{bmatrix}\mathbf{B}_{q_1,k} & \mathbf{0} & \cdots & \mathbf{0}\\ \mathbf{0} & \mathbf{B}_{q_2,k} & \cdots & \mathbf{0}\\ \vdots & \vdots & \ddots & \vdots\\ \mathbf{0} & \mathbf{0} & \cdots & \mathbf{B}_{q_d,k}\end{bmatrix} = \text{blkdiag}(\mathbf{B}_{q_1,k},\ldots,\mathbf{B}_{q_d,k}),$$

where $[\mathbf{B}_{q_i,k}]_{\varphi(q_i)\times\varphi(q_i)}$ is the channel matrix for subspace $\mathcal{S}_{q_i}$ with skew circulant matrix structure. By the orthogonality of Ramanujan subspaces, $\mathbf{G}_k = \mathbf{B}_{q_k,k}$, $\mathbf{G}_{j,k} = \mathbf{0}$, $\forall j \neq k$. Thus, RPDMA achieves *zero inter-user interference*, and the extracted signal for user k becomes

$$\bar{\mathbf{y}}_k = \mathbf{M}_k^T\bar{\mathbf{y}} = \sqrt{\frac{P_k}{\varphi(q_k)}}\mathbf{B}_{q_k,k}\mathbf{d}_k + \bar{\mathbf{w}}_k$$

where $\mathbf{B}_{q_k,k} \in \mathbb{C}^{\varphi(q_k)\times\varphi(q_k)}$ is the effective channel matrix for $\mathcal{S}_{q_k}$ and $\bar{\mathbf{w}}_k \sim \mathcal{CN}(\mathbf{0}, \sigma^2\mathbf{I}_{\varphi(q_k)})$. The block diagram representation of the RPDMA transmitter and receiver is illustrated in Fig. 1. In subsection III-C, we generalize this view using Nested Periodic Matrices (NPMs) and define the resulting NPDMA framework, for which OFDMA and RPDMA arise as special cases.

2) Illustrative Example

Consider an RPDMA system with $N = 4$ and divisors $\mathcal{D}_4 = \{1, 2, 4\}$. Suppose user k is assigned divisor $q_k = 4$, corresponding to the $\varphi(4) = 2$ dimensional $\mathcal{S}_4$. In this setting, the orthonormal matrix is:

$$[\mathbf{T}_{\text{NRPT}}]_{4\times4} = \begin{bmatrix}0.5 & 0.5 & \frac{1}{\sqrt{2}} & 0\\ 0.5 & -0.5 & 0 & \frac{1}{\sqrt{2}}\\ 0.5 & 0.5 & -\frac{1}{\sqrt{2}} & 0\\ 0.5 & -0.5 & 0 & -\frac{1}{\sqrt{2}}\end{bmatrix}.$$

The mapping matrix $\mathbf{M}_k$ selects the symbol vector $\mathbf{d}_k = [d_{k1}, d_{k2}]^T$ to the global basis as $\bar{\mathbf{x}}_k = \mathbf{M}_k\mathbf{d}_k = [0, 0, d_{k1}, d_{k2}]^T$. Assume user k's channel impulse response $\mathbf{h}_k = [0.8, 0.6]^T$ ($L = 2$). The circulant channel matrix $\mathbf{H}_{\text{cir},k}$ transforms under the normalized RPT as

$$\mathbf{T}_{\text{NRPT}}^T\mathbf{H}_{\text{cir},k}\mathbf{T}_{\text{NRPT}} = \text{blkdiag}\left(\underbrace{[1.4]}_{\mathbf{B}_{1,k}}, \underbrace{[0.2]}_{\mathbf{B}_{2,k}}, \underbrace{\begin{bmatrix}0.8 & -0.6\\ 0.6 & 0.8\end{bmatrix}}_{\mathbf{B}_{4,k}}\right).$$

The received signal for user k becomes $\bar{\mathbf{y}}_k = \sqrt{\frac{P_k}{2}}\,\mathbf{B}_{4,k}\mathbf{d}_k + \bar{\mathbf{w}}_k$, where $\bar{\mathbf{w}}_k \sim \mathcal{CN}(\mathbf{0}, \sigma^2\mathbf{I}_2)$. Crucially, there is *zero interference* from users in $\mathcal{S}_1$ or $\mathcal{S}_2$ due to the orthogonal subspace structure.

3) Frequency Diversity and Diversity Order

The frequency diversity in RPDMA arises from the spectral structure of Ramanujan subspaces. For a divisor q_k, the basis functions in $\mathcal{S}_{q_k}$, i.e., $c_{q_k}(n)$ and its circular shifts, have DFTs with exactly $\varphi(q_k)$ non-zero components located at

$$\mathcal{B}_{q_k} = \left\{\left(\frac{kN}{q_k}\right) \bmod N \,\middle|\, 1 \le k \le q_k,\ (k, q_k) = 1\right\},$$

which are non-adjacent and spaced by at least N/q_k bins. In the dyadic case $N = 2^m$, we have $|\mathcal{B}_{q_k}| = \varphi(q_k) = q_k/2$, and the family $\{\mathcal{B}_q\}_{q|N}$ forms a disjoint partition of $\{0, 1, \ldots, N-1\}$. In the proposed RPDMA scheme, each symbol in $\mathbf{d}_k$ distributes its energy across the $\varphi(q_k)$ non-adjacent frequencies in $\mathcal{B}_{q_k}$. The following theorem formalizes the corresponding diversity order.

Theorem 1 (Frequency diversity order of RPDMA): Consider user k assigned to the subspace $\mathcal{S}_{q_k}$ in the uplink system of Section III-A, with an L-tap frequency-selective

channel modeled by the circulant matrix $\mathbf{H}_{\mathrm{cir},k}$ in (6), whose taps are i.i.d. $\mathcal{CN}(0,1)$. Let $H_k(n)$ denote the N-point DFT of the channel impulse response, and collect the $\varphi(q_k)$ components indexed by $\mathcal{B}_{q_k}$ in $\mathbf{H}_{q_k} \triangleq \left[H_k(n)\right]_{n\in\mathcal{B}_{q_k}} \in \mathbb{C}^{\varphi(q_k)\times 1}$. Then the available frequency diversity order for user k is $d_k = \min\left\{\varphi(q_k),\, L\right\}$.

The proof is given in the Appendix. Theorem 1 shows that RPDMA can exploit up to $d_k = \min\{\varphi(q_k), L\}$ independent frequency dimensions per symbol. When $\varphi(q_k) \geq L$, user k attains the full L-tap frequency diversity offered by the channel, whereas for smaller subspaces the diversity order increases linearly with $\varphi(q_k)$. Therefore, RPDMA achieves an inherent frequency diversity without requiring explicit coding like SC-FDMA [8] and SLM in OFDM [17].

4) Computational Complexity Analysis

We now provide a detailed computational complexity analysis of the proposed RPDMA scheme, quantifying the number of Real Multiplications (RM) and Additions (RA) required at both the transmitter and receiver. The analysis leverages the unique sparse structure of $\mathbf{T}_{\mathrm{NRPT}}$ for $N = 2^m$ and the properties of the effective channel matrices.

Transmitter Complexity: At the transmitter, each user k performs two primary operations: subcarrier mapping and RPT modulation. The subcarrier mapping operation $\bar{\mathbf{x}}_k = \mathbf{M}_k\mathbf{d}_k$ is a simple selection process that requires no arithmetic operations. The subsequent RPT modulation $\mathbf{T}_{\mathrm{NRPT}}\bar{\mathbf{x}}_k$ is highly efficient due to the sparsity of $\mathbf{T}_{\mathrm{NRPT}}$. Crucially, each row of $\mathbf{T}_{\mathrm{NRPT}}$ contains exactly $\log_2 N + 1$ non-zero elements, and only one of these corresponds to the user's assigned subspace $\mathcal{S}_{q_k}$. Consequently, generating the time-domain signal for user k requires exactly $2N$ RM and no additional RA for the matrix–vector product itself. Prior to this, scaling the symbol vector $\mathbf{d}_k$ by $\sqrt{P_k/\varphi(q_k)}$ requires $4\varphi(q_k)$ RM and $2\varphi(q_k)$ RA. Therefore, the per-user transmitter complexity for RPDMA is $2N + 4\varphi(q_k)$ RM and $2\varphi(q_k)$ RA, which is $\mathcal{O}(N)$. The total transmitter complexity for all K users is $\mathcal{O}(KN)$, which, given $K \leq m+1 = \log_2 N + 1$, is $\mathcal{O}(N\log_2 N)$.

In an OFDMA transmitter, user k maps its data symbols onto N_k allocated subcarriers and performs modulation using an N-point Inverse Fast Fourier Transform (IFFT). Although the IFFT is computationally efficient, it operates on the full N-length vector irrespective of the number of allocated subcarriers. As a result, the per-user transmitter complexity of OFDMA is $\mathcal{O}(N\log_2 N)$, corresponding to approximately $2N\log_2 N$ RM and $3N\log_2 N$ RA. For a system with K users, the total transmitter complexity therefore scales as $\mathcal{O}(KN\log_2 N)$.

In SC-FDMA, the transmitter follows a similar processing chain to OFDMA [9], but includes an additional DFT precoding stage of size $\varphi(q_k)$ before subcarrier mapping and the N-point IFFT. The $\varphi(q_k)$-point DFT precoder can be implemented using FFT, which requires approximately $2\varphi(q_k)\log_2\varphi(q_k)$ RM and $3\varphi(q_k)\log_2\varphi(q_k)$ RA. Together with the N-point IFFT, the per-user SC-FDMA transmitter complexity for user k becomes $\left(2N\log_2 N + 2\varphi(q_k)\log_2\varphi(q_k)\right)$ RM and $\left(3N\log_2 N + 3\varphi(q_k)\log_2\varphi(q_k)\right)$ RA which is still $\mathcal{O}(N\log_2 N)$ since $\varphi(q_k) \leq N$. For a system with K users, the total SC-FDMA transmitter complexity is $\left(2KN\log_2 N + 2\sum_{k=1}^{K}\varphi(q_k)\log_2\varphi(q_k)\right)$ RM and $\left(3KN\log_2 N + 3\sum_{k=1}^{K}\varphi(q_k)\log_2\varphi(q_k)\right)$ RA which scales as $\mathcal{O}(KN\log_2 N)$ overall.

Receiver Complexity: At the base station, the RPDMA receiver first performs a global RPT demodulation, $\bar{\mathbf{y}} = \mathbf{T}_{\mathrm{NRPT}}^T\mathbf{y}$. Leveraging the matrix sparsity, this operation requires $2N(\log_2 N + 1)$ RM and $2N\log_2 N$ RA, resulting in a complexity of $\mathcal{O}(N\log_2 N)$. The signal for each user k is then extracted via the projection $\bar{\mathbf{y}}_k = \mathbf{M}_k^T\bar{\mathbf{y}}$, which involves no arithmetic computations. The final step is equalization to solve $\bar{\mathbf{y}}_k = \sqrt{P_k/\varphi(q_k)}\mathbf{B}_{q_k,k}\mathbf{d}_k + \bar{\mathbf{w}}_k$. Exploiting the skew-circulant structure of $\mathbf{B}_{q_k,k}$ with an FFT-based solver results in a per-user equalizer complexity of $\mathcal{O}(\varphi(q_k)\log_2\varphi(q_k))$, specifically $4\varphi(q_k)\log_2\varphi(q_k) + 4\varphi(q_k)$ RM and $6\varphi(q_k)\log_2\varphi(q_k) + 2\varphi(q_k)$ RA. The total receiver complexity is $\mathcal{O}(N\log_2 N + \sum_{k=1}^{K}\varphi(q_k)\log_2\varphi(q_k))$.

At the OFDMA receiver, the processing starts with a single N-point FFT applied to the received signal, which has a computational complexity of $\mathcal{O}(N\log_2 N)$. The receiver then performs subcarrier demapping for each user through a simple selection operation. For Linear Time Invariant (LTI), OFDMA results in single-tap equalizers, which is a per-subcarrier scalar operation, resulting in a per-user equalizer complexity of $\mathcal{O}(1)$. Each subcarrier equalization requires approximately 6 real multiplications (RMs) and 2 real additions (RAs), leading to a total receiver complexity of $\mathcal{O}(N\log_2 N + N)$. In SC-FDMA, the receiver follows the same processing steps as OFDMA but includes an additional IDFT post-processing stage of size $\varphi(q_k)$. Hence, for k^{th} user the IDFT complexity is $\mathcal{O}(\varphi(q_k)\log_2\varphi(q_k))$. Summing over all K users and using $\sum_{k=1}^{K}\varphi(q_k) = N$, the overall SC-FDMA receiver complexity becomes $\mathcal{O}\big(N\log_2 N + \sum_{k=1}^{K}\varphi(q_k)\log_2\varphi(q_k)\big)$.

Complexity Comparison: The computational load of all schemes is summarized in Table 1 for $N = 2^m$. From which we draw the following conclusions:

- *Comparison with OFDMA:* RPDMA reduces the per-user transmitter complexity to $\mathcal{O}(N)$ compared to OFDMA's $\mathcal{O}(N\log N)$. This lower complexity eases the computational load on user devices. Since $\sum_{k=1}^{K}\varphi(q_k)\log_2\varphi(q_k) > N$, RPDMA results in higher receiver computational complexity than OFDMA, which benefits from single-tap equalization.
- *Comparison with SC-FDMA:* RPDMA achieves lower transmitter complexity than SC-FDMA while maintaining comparable receiver complexity.

TABLE 1. Computational complexity of OFDMA, SC-FDMA, and RPDMA for $N = 2^m$.

Metric	RPDMA	OFDMA	SC-FDMA
Per-User Transmitter Complexity	$\mathcal{O}(N)$	$\mathcal{O}(N \log_2 N)$	$\mathcal{O}(N \log_2 N)$
Total Transmitter Complexity	$\mathcal{O}(N \log_2 N)$	$\mathcal{O}(KN \log_2 N)$	$\mathcal{O}(KN \log_2 N)$
Per-User Equalizer Complexity	$\mathcal{O}(\varphi(q_k) \log_2 \varphi(q_k))$	$\mathcal{O}(1)$	$\mathcal{O}(1)$
Total Receiver Complexity	$\mathcal{O}\big(N \log_2 N + \sum_{k=1}^{K} \varphi(q_k) \log_2 \varphi(q_k)\big)$	$\mathcal{O}(N \log_2 N + N)$	$\mathcal{O}\big(N \log_2 N + \sum_{k=1}^{K} \varphi(q_k) \log_2 \varphi(q_k)\big)$

C. NPDMA

In this subsection, we show that both OFDMA and RPDMA belong to a unified framework called *NPDMA*, characterized by the use of NPMs for modulation and demodulation. From a system perspective, NPDMA can be viewed as the generic version of the architecture in Fig. 1: each user k is assigned to a Nested Periodic Subspace (NPS) $\mathcal{P}_{q_k}$, its data vector $\mathbf{d}_k$ is first placed into the corresponding coordinates via $\mathbf{M}_k$, and a common NPM $\mathbf{T}$ (implemented by the "MCM" block $\mathbf{E}_m$) maps all users' symbols to the time-domain signal. At the base station, the inverse transform $\mathbf{T}^{-1}$ (the "MC Demodulation" block $\mathbf{E}_d$), followed by demapping with $\mathbf{M}_k^T$, recovers each user's signal for subsequent equalization and decoding. Different choices of $\mathbf{T}$ therefore generate different MA schemes within the same architecture.

Definition 1 (NPM [54]):
Consider the divisor set $\mathcal{D}_N = \{q_1, q_2, \ldots, q_d\}$. A matrix $\mathbf{T} \in \mathbb{C}^{N \times N}$ is called an NPM if it can be expressed as $\mathbf{T} = \left[\mathbf{T}_{q_1}, \mathbf{T}_{q_2}, \ldots, \mathbf{T}_{q_d}\right]$, and satisfies the following conditions: 1) Each submatrix $\mathbf{T}_{q_i} \in \mathbb{C}^{N \times \varphi(q_i)}$ has rank $\varphi(q_i)$. The $\varphi(q_i)$-dimensional subspace spanned by $\mathbf{T}_{q_i}$ is called NPS, denoted as $\mathcal{P}_{q_i}$. 2) $\mathbf{T}$ is a full-rank matrix. 3) Each column of $\mathbf{T}_{q_i}$ is a q_i-periodic sequence.

From (7), the period of the k^{th} column is $\frac{N}{(k,N)}$, which is always a divisor of N. For each divisor $q_i \in D_N$, the number of columns in $\mathbf{T}_{\text{NDFT}}$ having period exactly q_i is $\varphi(q_i)$. Let $\mathbf{T}_{q_i}$ is the submatrix constructed using these $\varphi(q_i)$ linearly independent columns. Since $\sum_{q_i|N} \varphi(q_i) = N$, the columns of $\mathbf{T}_{\text{NDFT}}$ can be partitioned into submatrices as $\mathbf{T}_{\text{NDFT}} = \left[\mathbf{T}_{q_1}, \mathbf{T}_{q_2}, \ldots, \mathbf{T}_{q_d}\right]$. By orthogonality and periodicity of the DFT basis, $\mathbf{T}_{\text{NDFT}}$ satisfies all conditions of an NPM. Therefore, the DFT matrix is a member of the NPM family. Similarly, one can verify that $\mathbf{T}_{\text{NRPT}}$ also lies within the NPM family. In addition to the DFT and RPT, other transforms such as the Complex Conjugate Periodic Transform (CCPT) [55]–[57], Orthogonal CCPT (OCCPT) [42], [58], Natural Basis Matrices (NBMs) [54], and Random Periodic Matrices (RPMs) [54] are also members of the NPM family.

1) NPDMA Transmitter and Receiver Design

Consider an NPM $\mathbf{T}$. In NPDMA, each user k is assigned to an NPS, $\mathcal{P}_{q_k}$. Thus, the NPDMA scheme exploits the structural properties of $\mathbf{T}$ to enable user multiplexing. In this setting, the NPDMA transmit signal is given by $\mathbf{x}_k = \sqrt{\frac{P_k}{\varphi(q_k)}}\mathbf{T}\mathbf{M}_k\mathbf{d}_k$, where $\mathbf{M}_k$ maps $\mathbf{d}_k$ to the indices of subcarriers belong to $\mathcal{P}_{q_k}$. At the base station, user k's data is obtained as:

$$\bar{\mathbf{y}}_k = \underbrace{\sqrt{\frac{P_k}{\varphi(q_k)}}\tilde{\mathbf{B}}_{q_k,k}\mathbf{d}_k}_{\text{desired signal}} + \underbrace{\sum_{j \neq k} \sqrt{\frac{P_j}{\varphi(q_j)}}\tilde{\mathbf{B}}_{q_k,j}\mathbf{d}_j}_{\text{inter-user interference}} + \bar{\mathbf{w}}_k, \quad (14)$$

where $\tilde{\mathbf{B}}_{q_k,j} = \mathbf{M}_k^T\mathbf{T}^{-1}\mathbf{H}_{\text{cir},j}\mathbf{T}\mathbf{M}_j$. When $\mathbf{T} = \mathbf{T}_{\text{DFT}}$ or $\mathbf{T}_{\text{NRPT}}$, the subspaces $\{\mathcal{P}_{q_i}\}_{q_i|N}$ reduce to $\{\mathcal{S}_{q_i}\}_{q_i|N}$ [54]. In this case, $\tilde{\mathbf{B}}_{q_k,j} = \mathbf{0}$ for $j \neq k$, eliminating inter-user interference. For non-orthogonal NPMs (e.g., CCPT, NBMs, and RPMs), inter-user interference arises due to $\tilde{\mathbf{B}}_{q_k,j} \neq \mathbf{0}$. In such cases, advanced interference cancellation or detection schemes are required at the receiver. In this work, we focus on OFDMA and RPDMA, with the following sections presenting both theoretical and numerical analyses of their PAPR performance.

IV. PAPR Analysis

In an MA system, the PAPR for user k is defined as

$$\text{PAPR}_k = \frac{\max\limits_{0 \leq n \leq N-1} |x_k(n)|^2}{\mathbb{E}\left[|x_k(n)|^2\right]}, \quad (15)$$

where $x_k(n)$ is the n^{th} sample of user k's signal $\mathbf{x}_k$ (5). Let the average power of an M-QAM symbol be $\alpha^2 = \mathbb{E}[|d_k(\cdot)|^2]$ and the worst-case peak power occurs for the corner symbol $\beta = (\sqrt{M}-1) + j(\sqrt{M}-1)$ with $|\beta|^2 = 2(\sqrt{M}-1)^2$. With this setting, we have the following theorem.

Theorem 2 (Worst-Case PAPR (WC-PAPR)):
Let $N = 2^m$ with $m \in \mathbb{N}$. Consider user k with modulated signal $\mathbf{x}_k$ derived from an uncorrelated M-QAM data vector $\mathbf{d}_k$. Then:

1) In OFDMA with N_k subcarriers allocated to user k:

$$\text{WC-PAPR}_{\text{OFDMA},k} = \frac{\frac{P_k N_k |\beta|^2}{N}}{\frac{P_k \alpha^2}{N}} = N_k \frac{|\beta|^2}{\alpha^2}. \quad (16)$$

2) In RPDMA with user k assigned to $\mathcal{S}_{q_k}$:

$$\text{WC-PAPR}_{\text{RPDMA},k} = \frac{\frac{P_k |\beta|^2}{N}}{\frac{P_k \alpha^2}{N}} = \frac{|\beta|^2}{\alpha^2}. \quad (17)$$

The proof is given in the Appendix. Notably, while the peak power in OFDMA scales linearly with N_k, the peak power in RPDMA remains independent of $\varphi(q_k)$. In both cases, however, the average power remains the same.

Remark: Theorem 2 characterizes the *deterministic* WC-PAPR under the amplitude constraint $|d_k(i)| \le |\beta|$, which is attained when all symbols take the corner value β. This configuration is extremely unlikely for random M-QAM data, so the resulting WC-PAPR values should be interpreted as conservative upper bounds rather than typical operating points. Later, we complement this result with probabilistic WC-PAPR bounds based on Hoeffding's inequality and with Complementary Cumulative Distribution Function (CCDF) versus PAPR simulations that capture the statistical behavior under i.i.d. M-QAM signaling.

In Theorem 2, the derivation of the WC-PAPR assumes $\alpha^2 = \mathbb{E}[|d_k(\cdot)|^2]$, which holds under the idealized assumption of infinitely long symbol sequences. However, practical implementations with finite symbol sequences may experience deviations between the empirical average power $\widehat{\alpha}^2$ and the theoretical value α^2. This mismatch leads to a gap between theoretical WC-PAPR predictions and simulation results. To overcome this issue, we employ concentration inequalities, specifically Hoeffding's inequality [59], which provides a probabilistic bound on the deviation of the sample mean from its expected value.

Throughout this subsection, we model the entries of $\mathbf{d}_k$ as independent and identically distributed (i.i.d.) M-QAM symbols drawn uniformly from the constellation. Consequently, the random variables $X_i \triangleq |d_k(i)|^2,\ i = 1, \ldots, L_k$, are i.i.d., real-valued, and bounded as $0 \le X_i \le |\beta|^2$, with common mean $\mathbb{E}[X_i] = \alpha^2$. The empirical mean power is $\widehat{\alpha}^2 = \frac{1}{L_k}\sum_{i=1}^{L_k} X_i$. Thus, Hoeffding's inequality is applied directly to the sequence $\{X_i\}$ of squared symbol magnitudes, which satisfies the required independence and boundedness conditions. Hoeffding's inequality states that for any $\epsilon > 0$, the probability that $\widehat{\alpha}^2$ deviates from its expectation by more than ϵ is bounded as [59]

$$\Pr\left(\left|\widehat{\alpha}^2 - \alpha^2\right| \ge \epsilon\right) \ \le \ 2\exp\left(-\frac{2L_k\epsilon^2}{|\beta|^4}\right). \tag{18}$$

Here, ϵ is a deviation threshold. To obtain an explicit deviation bound for a desired confidence level $1-\delta$, we invert (18) by setting the right-hand side equal to δ, which yields

$$\epsilon(L_k, \delta) = |\beta|^2\sqrt{\frac{1}{2L_k}\ln\left(\frac{2}{\delta}\right)}. \tag{19}$$

Substituting this into (18), we obtain

$$\Pr\left(\alpha^2 - \epsilon(L_k,\delta) \ \le \ \widehat{\alpha}^2 \ \le \ \alpha^2 + \epsilon(L_k,\delta)\right) \ \ge \ 1-\delta,$$

which guarantees that the empirical mean power $\widehat{\alpha}^2$ remains within $\epsilon(L_k, \delta)$ of its expectation α^2 with probability at least $1-\delta$. In particular, this ensures with high confidence that the denominator of the WC-PAPR expression does not deviate too far from α^2. By extending this reasoning, we obtain:

Theorem 3 (Probabilistic WC-PAPR):

Let $N = 2^m$ and consider user k transmitting independent M-QAM data. Define the sample size

$$L_k \ = \ \begin{cases} N_k, & \text{(OFDMA)} \\ \varphi(q_k), & \text{(RPDMA).} \end{cases}$$

For confidence level $1-\delta$, where $\delta \in (0,1)$, with $\epsilon(L_k,\delta)$ defined in (19), if $\alpha^2 > \epsilon(L_k,\delta)$, then the empirical mean $\widehat{\alpha}^2$ satisfies

$$\widehat{\alpha}^2 \ \ge \ \alpha^2 - \epsilon(L_k,\delta)$$

with probability at least $1-\delta$. Consequently, the following probabilistic WC-PAPR upper bounds hold with probability at least $1-\delta$:

$$\text{WC-PAPR}_{\text{OFDMA},k}(\delta) \le \frac{N_k\,|\beta|^2}{\alpha^2 - \epsilon(N_k,\delta)}, \tag{20}$$

$$\text{WC-PAPR}_{\text{RPDMA},k}(\delta) \le \frac{|\beta|^2}{\alpha^2 - \epsilon(\varphi(q_k),\delta)}. \tag{21}$$

If $\alpha^2 \le \epsilon(L_k,\delta)$, then the bound becomes vacuous because the denominator in (20)–(21) is non-positive. In this case, one must relax the confidence level by choosing a larger δ.

Remark: Hoeffding's inequality applies to any collection of independent bounded random variables and does not require identical distributions. In scenarios where the symbol energies $\{|d_k(i)|^2\}$ are independent but not identically distributed, the same argument holds by defining $X_i = |d_k(i)|^2$ with possibly different means $\mathbb{E}[X_i]$ and replacing α^2 in Theorem 3 with the overall average $\mu = \frac{1}{L_k}\sum_{i=1}^{L_k}\mathbb{E}[X_i]$. In this paper, we focus on the i.i.d. case, which matches the simulation setup and simplifies notation.

This probabilistic WC-PAPR accounts for the deviation of the empirical average power from the expectation α^2 and establishes rigorous probabilistic bounds on the WC-PAPR of OFDMA and RPDMA. Table 2 summarizes the probabilistic WC-PAPR bounds for OFDMA and RPDMA with $N = 512$, as the active subspace dimension L_k varies. The Hoeffding correction appears in the form $\alpha^2 - \epsilon$, which serves as the effective lower bound on the empirical average power. The key observations are:

- As L_k increases, $\alpha^2 - \epsilon$ approaches the nominal mean power $\alpha^2 = 1$, resulting in progressively tighter WC-PAPR bounds.
- For OFDMA, WC-PAPR exhibits a rapid increase with L_k, reflecting its sensitivity to larger subspace sizes. In contrast, RPDMA shows a decay in WC-PAPR as L_k grows, highlighting its robustness against peak power fluctuations.
- The impact of the confidence level δ is evident: a smaller value ($\delta = 0.001$) yields more conservative WC-PAPR bounds compared to $\delta = 0.01$.
- Overall, the results confirm that RPDMA consistently outperforms OFDMA in terms of PAPR performance, even under probabilistic guarantees.

TABLE 2. Probabilistic WC-PAPR bounds of OFDMA and RPDMA with Hoeffding correction for different sample sizes L_k for $N = 512$.

L_k	Ideal WC-PAPR$_{\text{OFDMA}}$ (dB)	Ideal WC-PAPR$_{\text{RPDMA}}$ (dB)	$\delta = 0.01$			$\delta = 0.001$		
			$\alpha^2 - \epsilon$	WC-PAPR$_{\text{OFDMA}}$ (dB)	WC-PAPR$_{\text{RPDMA}}$ (dB)	$\alpha^2 - \epsilon$	WC-PAPR$_{\text{OFDMA}}$ (dB)	WC-PAPR$_{\text{RPDMA}}$ (dB)
16	14.59	2.55	0.2676	20.3196	8.2784	0.1227	23.7042	11.6630
32	17.60	2.55	0.4821	20.7729	5.7214	0.3797	21.8100	6.7585
64	20.61	2.55	0.6338	22.5951	4.5333	0.5614	23.1220	5.0602
128	23.62	2.55	0.7410	24.9264	3.8543	0.6898	25.2373	4.1652
256	26.63	2.55	0.8169	27.5135	3.4311	0.7807	27.7104	3.6280

V. Results

In this section, we numerically evaluate and compare the PAPR of OFDMA, SC-FDMA, and RPDMA. In practical wireless systems, user devices often exhibit highly diverse QoS requirements, ranging from delay-tolerant applications such as messaging and sensor updates to high-throughput services like voice calls, augmented reality, and ultra-HD video streaming [2]. Efficient MA schemes must therefore support flexible and QoS-aware resource allocation across heterogeneous users while maintaining favorable signal properties such as low PAPR for energy-efficient transmission. To accommodate these requirements, we consider two scenarios. Scenario 1 captures a baseline case where each user is assigned a single Ramanujan subspace, enabling a structured allocation aligned with incremental QoS levels. Scenario 2, on the other hand, represents a more practical setting in next-generation systems, where users with stringent QoS demands may need to aggregate multiple subspaces to meet their high data-rate and low-latency requirements. Together, these scenarios provide a meaningful framework for evaluating the robustness of RPDMA against OFDMA and SC-FDMA under QoS-driven resource allocation, thereby highlighting its potential in meeting the heterogeneous service demands of 5G/6G uplink IoT systems [60].

For a fair comparison, each k^{th} user in RPDMA, OFDMA, and SC-FDMA is assigned to the subcarrier set $\mathcal{S}_{q_k}$ and all unassigned subcarriers are set to zero, such that the number of subcarriers allocated to user k is $N_k = \varphi(q_k)$ with localized mapping within the N subcarriers. For each user, we compute the CCDF of the PAPR for $N = 256$ and $N = 512$ using 16-QAM modulation, based on 10^6 realizations of the MCM symbolsẆith this setup, we analyze the two scenarios below.

Scenario-1: In this scenario, users are assigned a single Ramanujan subspace according to their QoS requirements. Higher QoS users are allocated larger subspaces (i.e., more subcarriers). For example, in a system with $N = 256 = 2^8$ subcarriers, the set of divisors is $\mathcal{D}_{256} = \{1, 2, 4, 8, 16, 32, 64, 128, 256\}$, supporting up to nine users, each mapped to a distinct divisor subspace. Users are indexed in ascending order of QoS demand, so the k^{th} user has lower QoS than the $(k+1)^{\text{th}}$ user. Accordingly, User 9, with the highest QoS, is assigned $\mathcal{S}_{256}$ of dimension $\varphi(256) = 128$. Similarly, for $N = 512 = 2^9$, the system accommodates ten users. The subcarrier allocations for $N = 256$ and $N = 512$ are summarized in Table 3. Fig. 2 and Fig. 3 show CCDF versus PAPR for OFDMA, SC-FDMA, and RPDMA with $N = 256$ and $N = 512$, respectively. The performance of each user can be identified with the respective notions on top of each subplot in Fig. 2 and Fig. 3. Note that users 1 and 2 have low QoS requirements and are therefore assigned to $\mathcal{S}_1$ and $\mathcal{S}_2$, each containing only a single subcarrier. As a result, their corresponding PAPR values remain close to zero, independent of N, and are omitted for brevity. From these figures, we conclude that users 3 to 9 for $N = 256$ and users 3 to 10 for $N = 512$ RPDMA demonstrate superior PAPR performance compared to both OFDMA and SC-FDMA. In SC-FDMA, a DFT precoder of configurable size N_s precedes subcarrier mapping. To maintain the same SE, we considered the same subspace allocation with $N_s = \varphi(q_k)$ in SC-FDMA for both scenarios 1 and 2. Moreover, as the QoS requirement increases, the PAPR gap between OFDMA and SC-FDMA widens, typically by about 2–3 dB at a CCDF of 10^{-4}.

TABLE 3. Subcarrier mapping to users for $N = 256$ and $N = 512$.

q_k	1	2	4	8	16	32	64	128	256	512
$\varphi(q_k)$	1	1	2	4	8	16	32	64	128	256
Mapping Indices	0	1	2-3	4-7	8-15	16-31	32-63	64-127	128-255	256-511
k^{th} user ($N = 256$)	1	2	3	4	5	6	7	8	9	-
k^{th} user ($N = 512$)	1	2	3	4	5	6	7	8	9	10

TABLE 4. Divisor Subspaces Grouping For $N = 256$ and $N = 512$.

$N = 256$									
q_k	1	2	4	8	16	32	64	128	256
$\varphi(q_k)$	1	1	2	4	8	16	32	64	128
k^{th}	0-15 (Low QoS)					16-63 (Medium QoS)		64-255 (High QoS)	
Users	User 1(N_3=16)					User 2 (N_2=48)		User 3 (N_1=192)	
$N = 512$									
q_k	1	2	4	8	16	32	64	128	256 512
$\varphi(q_k)$	1	1	2	4	8	16	32	64	128 256
k^{th} User	0-31 (Low QoS)					32-127 (Medium QoS)		128-511(High QoS)	
Users	User 1 (N_3=32)					User 2 (N_2=96)		User 3 (N_1=384)	

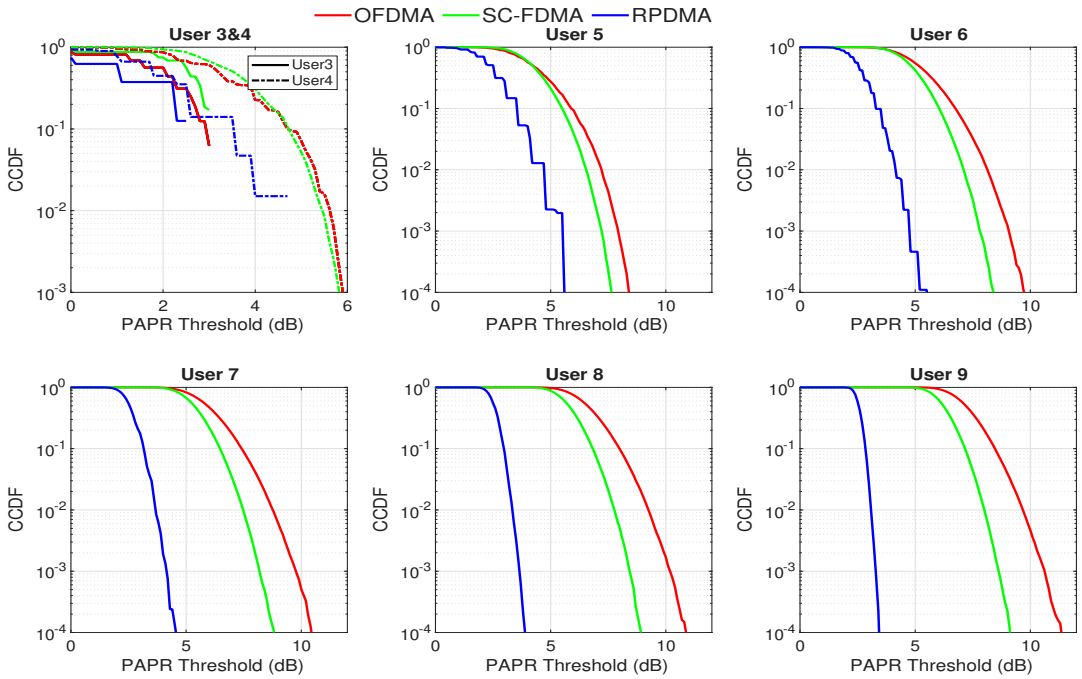

FIGURE 2. **Scenario 1: CCDF versus PAPR performance of OFDMA, RPDMA, and SC-FDMA for $N = 256$.**

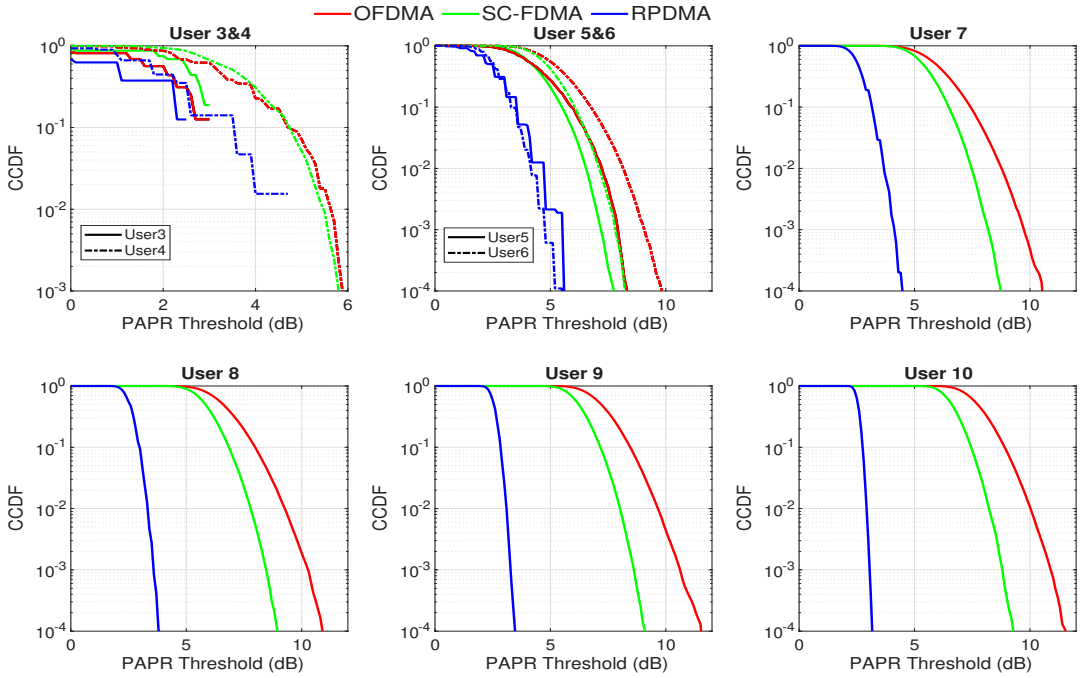

FIGURE 3. **Scenario 1: CCDF versus PAPR performance of OFDMA, RPDMA, and SC-FDMA for $N = 512$.**

This gap is less than conventional OFDM and SC-FDMA systems, which is typically 3–5 dB. This is because the same number of subcarriers is allocated to all OFDM, SC-FDMA, and RPDM systems. Nevertheless, RPDMA consistently achieves a lower PAPR than both schemes in these scenarios.

Additionally, Fig. 4a–4b show that OFDMA and SC-FDMA exhibit an increasing PAPR trend as the number of allocated subcarriers (subspace size) grows, whereas RPDMA generally shows a decreasing PAPR trend for users assigned to larger subspaces. For $N = 512$, at a CCDF of 10^{-3}, the RPDMA PAPR decreases from 4.8 dB (User 4) to 3.3 dB (User 10), while the corresponding values for OFDMA increase from 6.1 dB to 10.7 dB and for SC-FDMA from 5.8 dB to 8.7 dB, as seen in Fig. 4b.

It is worth noting that, for RPDMA, a slight non-monotonic behavior appears for Users 3–5. The PAPR first

This article has been accepted for publication in IEEE Open Journal of Vehicular Technology. This is the author's version which has not been fully edited and content may change prior to final publication. Citation information: DOI 10.1109/OJVT.2026.3661153

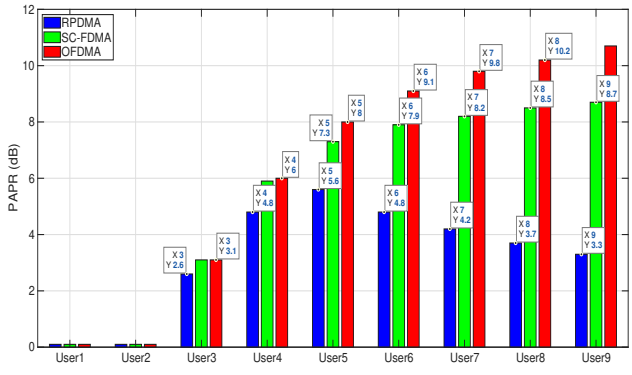

(a)

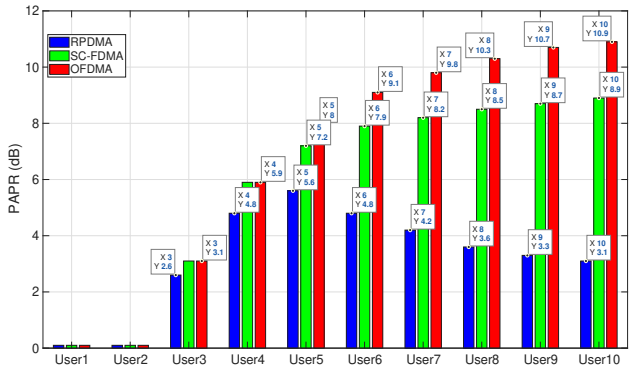

(b)

FIGURE 4. (a)-(b) Scenario 1: PAPR of RPDMA, SC-FDMA, and OFDMA for $N = 256$ and 512, respectively, at CCDF of 10^{-3}.

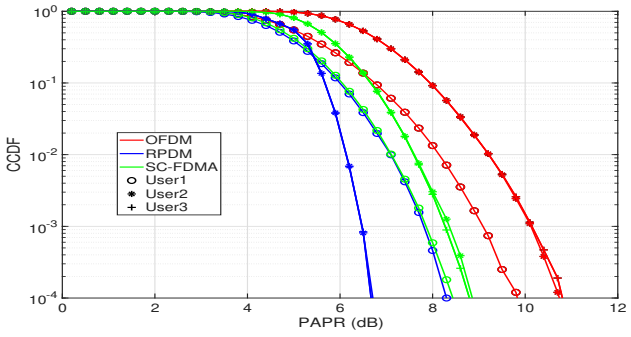

(a)

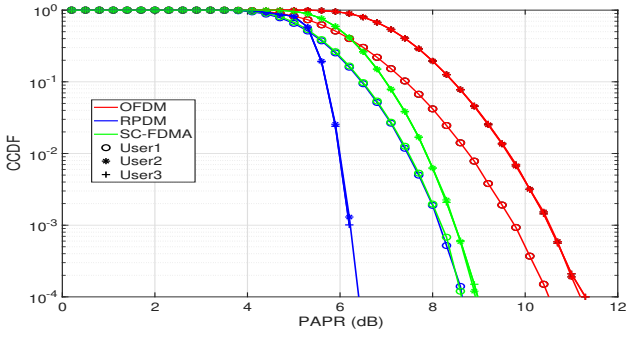

(b)

FIGURE 5. (a)-(b) Scenario 2: CCDF versus PAPR performance of OFDMA, SC-FDMA, and RPDMA for $N = 256$ and $N = 512$, respectively.

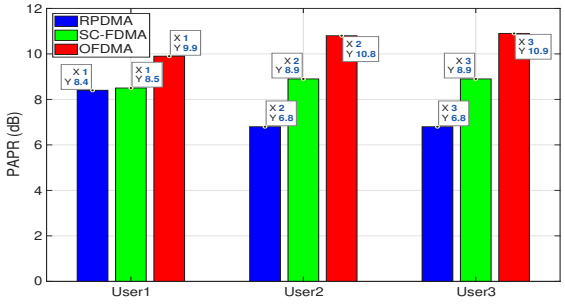

(a)

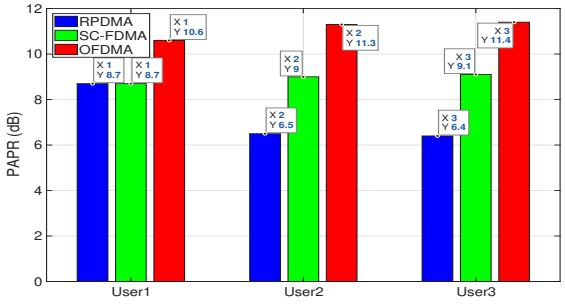

(b)

FIGURE 6. (a)-(b) Scenario 2: PAPR of RPDMA, SC-FDMA, and OFDMA for $N = 256$ and 512, respectively, at CCDF of 10^{-3}.

increases and then starts to decrease from User 6 onward. This is a finite-block-length effect: RPDMA's PAPR for user k is essentially the ratio of the largest symbol energy in the block to the empirical average symbol energy over $\varphi(q_k)$ QAM symbols. When $\varphi(q_k)$ is small (Users 3–5), this empirical average has high variance, and rare blocks containing one or more high-energy corner symbols together with several low-energy symbols can yield atypically large PAPR values. As $\varphi(q_k)$ increases (Users 6–10), the empirical average power concentrates around its nominal value α^2, stabilizing the denominator and causing the PAPR to decrease toward the bounded value $|\beta|^2/\alpha^2$, in agreement with the probabilistic WC-PAPR bounds in Table 2.

Scenario-2: Here, multiple subspaces are allocated to each user according to their QoS requirements. We illustrate this with three service types, each represented by an user:

- **User 3 (High QoS):** A high-definition video streaming user, requiring high data rates and low latency, is allocated 75% of the available subcarriers, i.e., $N_1 = \frac{3N}{4}$.
- **User 2 (Medium QoS):**A voice call user, requiring moderate data rates and low latency, is allocated 75% of the remaining subcarriers, i.e., $N_2 = \frac{3(N-N_1)}{4} = \frac{3N}{16}$.
- **User 1 (Low QoS):** A text messaging user, with minimal rate requirements and high delay tolerance, is allocated the remaining subcarriers, $N_3 = N - N_1 - N_2 = \frac{N}{16}$.

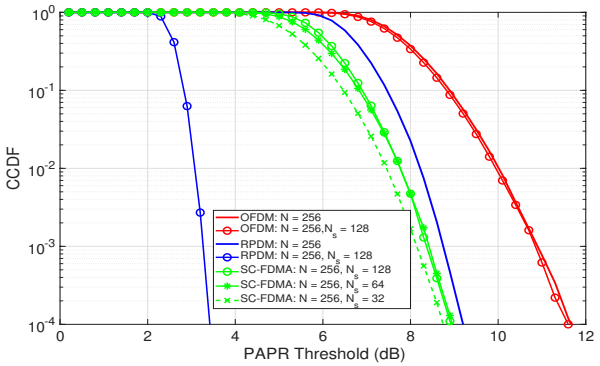

FIGURE 7. PAPR of OFDM, RPDM, and SC-FDMA for $N = 256$ with $N_s = \{32, 64, 128\}$ selected carriers

Thus, subcarriers are hierarchically allocated in a $3:1$ ratio, applied sequentially across QoS classes. The resulting user allocations for $N = 256$ and $N = 512$ are summarized in Table 4.

For Scenario 2, RPDMA again demonstrates superior PAPR performance compared to both OFDMA and SC-FDMA, as shown in Fig. 5a and Fig. 5b for $N = 256$ and 512, respectively. The trend of reduced PAPR with larger subspace sizes, observed in Scenario 1, is also valid for Scenario 2, which is consistently evident across all users, as shown in Fig. 6a and Fig. 6b. Notably, the PAPR values in both scenarios remain well within the theoretical bounds provided in Table 2.

Remark: In SC-FDMA, reducing the DFT size N_s, equal to the number of allocated data subcarriers, spreads each symbol across fewer subcarriers, which smooths the time-domain envelope and lowers PAPR. Fig. 7 plots the CCDF of PAPR for OFDMA, SC-FDMA, and RPDMA with $N = 256$; the SC-FDMA curves correspond to DFT sizes $N_s = 128$, 64, and 32. Relative to OFDMA, SC-FDMA achieves about $2 - 3\,\mathrm{dB}$ lower PAPR at a CCDF of 10^{-4}. Further reducing the DFT size offers diminishing returns; decreasing N_s from 128 to 32 yields little additional PAPR reduction, while incurring a loss in data rate and SE.

VI. SE and BER Analysis

To validate RPDMA further, in this Section, we analyze both SE and BER of RPDMA and compare them with those of OFDMA.

A. SE

We compare the achievable SE of OFDMA, SC-FDMA, and RPDMA for $N = 2^m$. In all schemes, user k is assigned to subcarriers in $\mathcal{S}_{q_k}$ such that $N_k = \varphi(q_k)$, i.e., in OFDMA and SC-FDMA we constrain $\mathcal{Q}_k = \mathcal{B}_{q_k}$. With Gaussian signaling, the instantaneous mutual information for user k is [53]

$$C_k = \log_2\Big[\det\Big(\mathbf{I}_{N_k} + \tfrac{P_k}{N_k\sigma^2}\,\mathbf{G}_k\mathbf{G}_k^H\Big)\Big] \quad \text{bits/channel-use}, \tag{22}$$

TABLE 5. OFDMA versus RPDMA for $N = 2^m$, $m \in \mathbb{N}$.

Feature	RPDMA	OFDMA
Basis	RSs (integer-valued)	Complex exponentials
Basis Orthogonality	Yes	Yes
User Allocation	Subspace-wise	Arbitrary
Max Users	$m+1$, $m = \log_2 N$	N
Inter-User Interference	None	None
User k Effective Channel Matrix	Skew-circulant	Diagonal
Frequency Diversity	Inherent	Requires coding
PAPR	Low	High
Transmitter Complexity	Low	High
Receiver Complexity	High	Low
Per-User Equalizer Complexity	$\mathcal{O}(\varphi(q_k)\log_2\varphi(q_k))$ (matrix inversion)	$\mathcal{O}(1)$ (scalar division)

and the ergodic capacity is $\bar{C}_k \triangleq \mathbb{E}[C_k]$. Here σ^2 is the per-complex-dimension AWGN variance, and $\mathbf{G}_k$ is the effective per-user channel after demodulation and user extraction.

OFDMA: Since the DFT diagonalizes circulant channels,

$$\bar{C}_k^{\mathrm{OFDMA}} = \mathbb{E}\left[\sum_{n\in\mathcal{B}_{q_k}} \log_2\Big(1 + \tfrac{P_k}{\varphi(q_k)\sigma^2}\,|H_k(n)|^2\Big)\right]. \tag{23}$$

Here $\mathbf{\Lambda}_k[\mathcal{B}_{q_k}] = \mathrm{diag}\big(\{H_k(n)\}_{n\in\mathcal{B}_{q_k}}\big)$ (refer to (8)) collects the per-bin frequency responses of the kth user's channel, restricted to the indices in $\mathcal{B}_{q_k}$.

SC-FDMA: In SC-FDMA, user k first applies an N_k-point unitary DFT precoder $\mathbf{F}_{N_k}$ to its data vector, and then maps the resulting symbols onto the same subcarrier set $\mathcal{B}_{q_k}$. After CP removal, an N-point FFT, and subcarrier demapping, the effective channel between the precoded symbols and the receiver input for user k is $\mathbf{G}_k^{\text{SC-FDMA}} = \mathbf{\Lambda}_k[\mathcal{B}_{q_k}]\,\mathbf{F}_{N_k}$, and after applying $\mathbf{F}_{N_k}^H$ at the receiver, the overall effective channel becomes

$$\tilde{\mathbf{G}}_k^{\text{SC-FDMA}} = \mathbf{F}_{N_k}^H\,\mathbf{\Lambda}_k[\mathcal{B}_{q_k}]\,\mathbf{F}_{N_k}.$$

Since $\mathbf{F}_{N_k}$ is unitary, the matrices $\tilde{\mathbf{G}}_k^{\text{SC-FDMA}}\tilde{\mathbf{G}}_k^{\text{SC-FDMA}H}$ and $\mathbf{\Lambda}_k[\mathcal{B}_{q_k}]\mathbf{\Lambda}_k^H[\mathcal{B}_{q_k}]$ have the same eigenvalues, and unitary invariance of the determinant in (22) yields

$$\bar{C}_k^{\text{SC-FDMA}} = \mathbb{E}\left[\sum_{n\in\mathcal{B}_{q_k}} \log_2\Big(1 + \tfrac{P_k}{\varphi(q_k)\sigma^2}\,|H_k(n)|^2\Big)\right]. \tag{24}$$

Thus, under Gaussian signaling and the same subcarrier set $\mathcal{B}_{q_k}$, SC-FDMA and OFDMA achieve the same ergodic capacity.

RPDMA: For $N = 2^m$, $\mathbf{T}_{\mathrm{NRPT}}$ is orthonormal. Using the selector $\mathbf{M}_k$ and the index set $\mathcal{B}_{q_k}$, the RPT basis restricted to $\mathcal{S}_{q_k}$ admits the unitary change of basis

$$\mathbf{T}_{\mathrm{NRPT}}\mathbf{M}_k = \mathbf{T}_{\mathrm{NDFT}}(:,\mathcal{B}_{q_k})\,\mathbf{U}_{q_k}, \tag{25}$$

This article has been accepted for publication in IEEE Open Journal of Vehicular Technology. This is the author's version which has not been fully edited and content may change prior to final publication. Citation information: DOI 10.1109/OJVT.2026.3661153

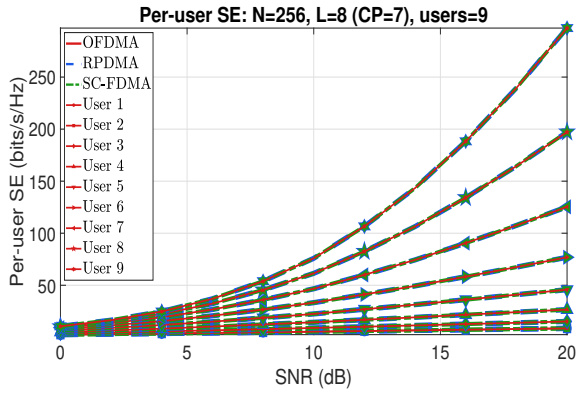

FIGURE 8. Per-user SE of OFDMA, SC-FDMA, and RPDMA with $N = 256$ for scenario-1.

where $\mathbf{U}_{q_k} \in \mathbb{C}^{\varphi(q_k)\times\varphi(q_k)}$ is unitary; explicitly, $\mathbf{U}_{q_k} = \mathbf{T}^H_{\mathrm{NDFT}}(:, \mathcal{B}_{q_k})\,\mathbf{T}_{\mathrm{NRPT}}\mathbf{M}_k$. Employing (25) simplifies (12) as $\mathbf{G}_k^{\mathrm{RPDMA}} = \mathbf{U}_{q_k}^H\,\mathbf{\Lambda}_k[\mathcal{B}_{q_k}]\,\mathbf{U}_{q_k}$, and unitary invariance of the determinant yields

$$\bar{C}_k^{\mathrm{RPDMA}} = \mathbb{E}\left[\sum_{n\in\mathcal{B}_{q_k}} \log_2\!\left(1 + \tfrac{P_k}{\varphi(q_k)\sigma^2}\,|H_k(n)|^2\right)\right]. \quad (26)$$

Accounting for the CP of length $L-1$, the per-user SE is

$$\eta_k^{(\cdot)} = \frac{N}{N+L-1}\,\bar{C}_k^{(\cdot)} \ \text{ bits/s/Hz}, \quad (27)$$

and the system SE is $\eta_{\mathrm{sum}}^{(\cdot)} = \sum_{k=1}^{K}\eta_k^{(\cdot)}$. From the above analysis, we state the following:

Theorem 4:
Let $N = 2^m$ and assign each user k a divisor subspace $\mathcal{S}_{q_k}$ where $q_k \mid N$ with $N_k = \varphi(q_k)$ in OFDMA, SC-FDMA, and RPDMA. Then, for every k, $\bar{C}_k^{\mathrm{OFDMA}} = \bar{C}_k^{\mathrm{SC\text{-}FDMA}} = \bar{C}_k^{\mathrm{RPDMA}}$ and $\eta_k^{\mathrm{OFDMA}} = \eta_k^{\mathrm{SC\text{-}FDMA}} = \eta_k^{\mathrm{RPDMA}}$. Hence $\eta_{\mathrm{sum}}^{\mathrm{OFDMA}} = \eta_{\mathrm{sum}}^{\mathrm{SC\text{-}FDMA}} = \eta_{\mathrm{sum}}^{\mathrm{RPDMA}}$.

To validate the theory, we consider scenario-1 with $N = 256$ and compute the per-user SE of both OFDMA and RPDMA for SNRs from 0 to 20 dB, as shown in Fig. 8. The user subspace assignment is given in Table 3. For simulation, we consider an i.i.d. Rayleigh channel with $L = 8$ taps, $\sigma^2 = 1$, $P_k = 1$, and average over 2000 channel realizations per SNR point. The simulated curves confirm that the per-user SE of OFDMA, SC-FDMA, and RPDMA is the same.

B. BER Analysis

This subsection numerically evaluates the uncoded BER performance of RPDMA, OFDMA, and SC-FDMA with $N = 256$ and $N = 512$ for Scenarios 1 and 2. We generate 10^5 bits, apply 16-QAM modulation, and perform multi-carrier modulation using all the above-mentioned schemes. Then the signal is transmitted over a quasi-static frequency-selective channel with $L = 8$ i.i.d. Rayleigh distribution (zero mean, unit variance) along with CP of length $L-1$. At the receiver, after removing the CP, Zero-Forcing (ZF) equalization is applied by assuming perfect CSI and synchronization without any hardware impairments to detect the final information of the users at the base station. Under this setup, sweeping SNR from 0 to 30 dB and for each SNR point, we run 100 Monte-Carlo trials. The results in Fig. 9a and Fig. 9b show that, at a BER of 10^{-4}, RPDMA improves performance over OFDMA by approximately 2.5dB, while SC-FDMA achieves about 5dB gain over OFDMA and 2dB over RPDMA. Additionally, allocating multiple Ramanujan subspaces to a user (see scenario-2) increases the BER.

Under the common CP-based framework described above, OFDMA with localized allocation maps each data symbol to an independent individual subcarrier, whereas RPDMA spreads each symbol across dependent subcarriers that offer diversity. This enables the exploitation of frequency diversity more effectively for RPDMA than OFDMA. As a result, RPDMA exhibits improved BER performance as SNR increases compared to OFDMA. In contrast, SC-FDMA with localized mapping and spreading introduced by DFT pre/post-coding distributes each user's symbols across multiple frequency components that achieves better diversity compared to OFDMA and RPDMA. Consequently, SC-FDMA offers better BER compared to both RPDMA and OFDMA. Here, we use the BER curves primarily as a sanity check rather than as a full BER analysis. A detailed analytical study of the BER performance of RPDMA, in both coded and uncoded settings, is an interesting topic on its own and will be pursued as future work.

VII. Discussion

Table 5 summarizes the key findings of this work and compares them with those of OFDMA. In summary, RPDMA has two critical advantages that are paramount for uplink scenarios: firstly, a lower per-user transmitter complexity, which reduces the computational burden on user equipment. Secondly, it provides low PAPR and inherent frequency diversity, eliminating the need for additional and complex coding schemes that OFDMA requires to achieve similar robustness. This makes RPDMA particularly advantageous for power-limited Internet of Things (IoT) and mobile devices, where energy efficiency is the primary design constraint. Beyond the presented results, several extensions are possible:

- **Limited number of users**: The RPDMA proposed in this work considers the subspace-wise user allocation, which restricts the maximum number of users to the number of divisors of N. To overcome this limitation, one could allow arbitrary user allocation, similar to OFDMA, by assigning multiple users within the same subspace. Additionally, multiple users share a complete subspace similar to the NOMA principle [5] instead of individual subcarriers. However, this inevitably introduces inter-user interference, necessitating efficient equalization strategies to separate user signals reliably.

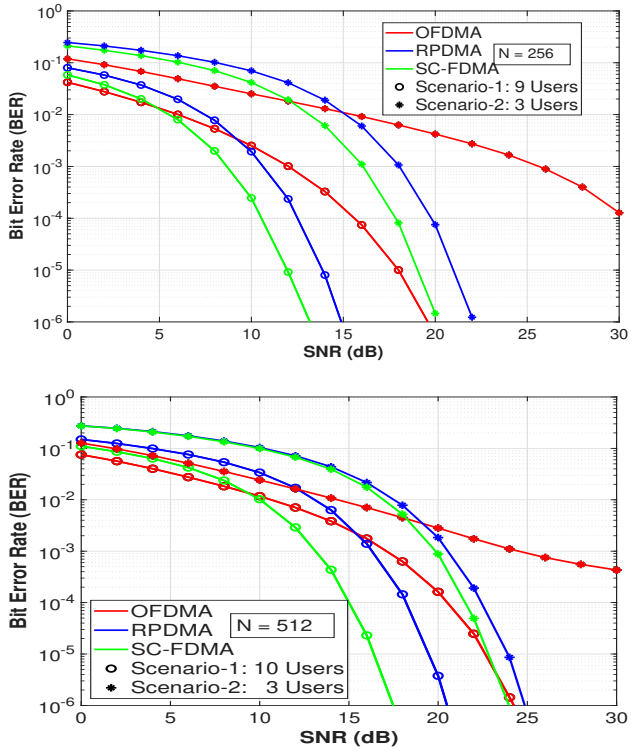

FIGURE 9. (a)-(b) BER of RPDMA, SC-FDMA, and OFDMA for $N = 256$ and 512.

We also anticipate that RPDMA could be combined with ML/DL–based receivers to further enhance performance and scalability; for example, multiple users multiplexed within the same Ramanujan subspace could be separated at the receiver using learned multi-user detectors, such as algorithm-unrolling networks inspired by sparse recovery. A detailed design and optimization of such hybrid RPDMA–ML architectures is left for future investigation.

- **Generality for arbitrary $N \in \mathbb{N}$:** The PAPR analysis in this paper was restricted to $N = 2^m$. A valuable extension is to investigate both the theoretical and numerical performance of RPDMA for arbitrary $N \in \mathbb{N}$, which would provide a more complete characterization of its applicability. Moreover, since the RPT matrix is not orthogonal when $N \neq 2^m$, computations become more demanding in such cases. This limitation can be mitigated by employing orthogonal Ramanujan bases as discussed in [61].
- **Practical Implementation Challenges:** RPDMA is a linear transformation–based waveform design, similar to OFDMA. As discussed in this work, both RPDMA and OFDMA belong to the family of NPDMA schemes. Therefore, existing synchronization and channel estimation techniques developed for OFDMA systems can be naturally extended to RPDMA. Nevertheless, a detailed investigation of these practical implementation challenges is left for future work.
- **Receiver Complexity Optimization:** While RPDMA reduces transmitter complexity, it increases receiver processing compared to OFDMA. This trade-off is well-suited to uplink scenarios where base stations have greater computational resources than user devices. However, reducing receiver complexity remains important for deployments with processing-constrained base stations. As mentioned in Section III-B, the effective channel matrix has a skew-circulant structure in RPDMA. Consequently, existing fast inverse computation algorithms for skew-circulant matrices may be exploited to reduce receiver complexity [62].

VIII. Conclusion

In this paper, we proposed a novel MA scheme, RPDMA, that extends RPDM to multi-user systems. We demonstrated that subspace-wise allocation ensures zero multi-user interference and provides inherent frequency diversity. We demonstrated through analytical derivations that RPDMA achieves lower PAPR than OFDMA for subcarrier sizes $N = 2^m$. We further analyzed computational complexity and showed that RPDMA reduces transmitter complexity at the expense of moderately higher receiver complexity. We introduced a generalized framework, NPDMA, which includes both RPDMA and OFDMA as special cases. We validated our analysis through simulations, which confirmed that RPDMA significantly outperforms OFDMA and SC-FDMA in terms of PAPR performance, especially for users assigned higher-dimensional subspaces. Finally, we showed that the SE of RPDMA matches that of OFDMA and SC-FDMA, and the BER simulation results reveal that SC-FDMA attains a lower BER than both alternatives, while RPDMA outperforms OFDMA as the SNR increases. Although SC-FDMA shows better BER performance, the inherent diversity, low PAPR characteristics, and lower transmitter computational complexity of RPDMA makes it as a promising candidate for next-generation uplink wireless systems.

Appendix

Proof of Theorem 1: Since the channel is circulant after CP removal (see Section III-A), its N-point DFT diagonalizes the convolution, and

$$H_k(n) = \sum_{\ell=0}^{L-1} h_k(\ell)\, e^{-j2\pi n\ell/N}, \quad 0 \le n \le N-1.$$

Stacking the entries for $n \in \mathcal{B}_{q_k}$ gives $\mathbf{H}_{q_k} = \mathbf{F}_{q_k}\, \mathbf{h}_k$, where $\mathbf{h}_k \in \mathbb{C}^{L\times 1}$ is the channel impulse response and $\mathbf{F}_{q_k} \in \mathbb{C}^{\varphi(q_k)\times L}$ has (i,ℓ)-th entry $e^{-j2\pi n_i \ell/N}$ with $n_i \in \mathcal{B}_{q_k}$. Thus, $\mathbf{F}_{q_k}$ is a (truncated) Vandermonde matrix evaluated at distinct frequency points; its rank is $\mathrm{rank}(\mathbf{F}_{q_k}) = \min\{\varphi(q_k), L\}$. Hence $\mathbf{H}_{q_k}$ lies in an r_k-dimensional subspace with $r_k \triangleq \mathrm{rank}(\mathbf{F}_{q_k}) = \min\{\varphi(q_k), L\}$, so there are r_k statistically independent fading coefficients across the $\varphi(q_k)$ frequencies in $\mathcal{B}_{q_k}$. From the RPDMA input–output

relation

$$\bar{\mathbf{y}}_k = \sqrt{\tfrac{P_k}{\varphi(q_k)}}\,\mathbf{B}_{q_k,k}\mathbf{d}_k + \bar{\mathbf{w}}_k,$$

each symbol in $\mathbf{d}_k$ is linearly spread across all entries of $\mathbf{H}_{q_k}$ via a unitary transform. Consequently, each symbol effectively experiences r_k independently faded components; we therefore take $d_k = r_k = \min\{\varphi(q_k), L\}$ as the available frequency diversity order for user k.

Proof of Theorem 2: OFDMA Derivation- The time-domain signal for user k is

$$x_k(n) = \sqrt{\frac{P_k}{N_k N}} \sum_{i\in\mathcal{Q}_k} d_k(i) e^{j2\pi i n/N}. \tag{28}$$

The WC-PAPR occurs when all $d_k(i) = \beta$ and at $n = 0$

$$\max_n |x_k(n)|^2 = \frac{P_k|\beta|^2}{N_k N}\left|\sum_{i\in\mathcal{Q}_k} 1\right|^2 = \frac{P_k N_k|\beta|^2}{N}. \tag{29}$$

Employing the uncorrelated nature of M-QAM symbols, the average power is

$$\mathbb{E}[|x_k(n)|^2] = \frac{P_k}{N_k N}\sum_{i\in\mathcal{Q}_k}\mathbb{E}\left\{|d_k(i)|^2\right\} = \frac{P_k\alpha^2}{N}. \tag{30}$$

Using (29) and (30), we get (16).

RPDMA Derivation- The time-domain signal for user k is synthesized as

$$x_k(n) = \sqrt{\frac{P_k}{\varphi(q_k)}}\sum_{l=0}^{\varphi(q_k)-1} d_k(l)\,\bar{c}^{(l)}_{q_k}(n), \tag{31}$$

where $\bar{c}^{(l)}_{q_k}(n) = \frac{1}{\sqrt{N\varphi(q_k)}} c_{q_k}(n-l)$ are normalized basis functions. The WC-PAPR occurs when all $d_k(l) = \beta$ and at $n = 0$

$$\max_n |x_k(n)|^2 = \frac{P_k|\beta|^2}{\varphi(q_k)}\left|\sum_{l=0}^{\varphi(q_k)-1}\bar{c}^{(l)}_{q_k}(l)\right|^2 \tag{32}$$

$$= \frac{P_k|\beta|^2}{\varphi(q_k)}\left(\frac{1}{\sqrt{N\varphi(q_k)}}\sum_{l=0}^{\varphi(q_k)-1} c_{q_k}(l)\right)^2. \tag{33}$$

For $q_k = 2^r$, $r \in \mathbb{N}$, the RS satisfies $\sum_{l=0}^{\varphi(q_k)-1} c_{q_k}(l) = \varphi(q_k)$. This implies

$$\max_n |x_k(n)|^2 = \frac{P_k|\beta|^2}{\varphi(q_k)}\left(\frac{\varphi(q_k)}{\sqrt{N\varphi(q_k)}}\right)^2 = \frac{P_k|\beta|^2}{N}. \tag{34}$$

Using the uncorrelated nature of M-QAM symbols, the average power is

$$\mathbb{E}[|x_k(n)|^2] = \frac{P_k}{\varphi(q_k)}\sum_{l=0}^{\varphi(q_k)-1}\mathbb{E}[|d_k(l)|^2]\,|\bar{c}^{(l)}_{q_k}(n)|^2 \tag{35}$$

$$= \frac{P_k\alpha^2}{N\varphi^2(q_k)}\sum_{l=0}^{\varphi(q_k)-1}|c_{q_k}(n-l)|^2. \tag{36}$$

For $q_k = 2^r$, we have $\sum_{l=0}^{\varphi(q_k)-1}|c_{q_k}(n-l)|^2 = \varphi^2(q_k)$. Using this, we get

$$\mathbb{E}[|x_k(n)|^2] = \frac{P_k\alpha^2}{N}. \tag{37}$$

Leveraging (34) and (37), we get (17).

REFERENCES

[1] D. K. Sah, M. Vahabi, and H. Fotouhi, "A comprehensive review on 5g iiot test-beds," *IEEE Transactions on Consumer Electronics*, vol. 71, no. 2, pp. 4139–4163, 2025.

[2] Z. Jiang, S. Zhou, and Z. Niu, "Distributed policy learning based random access for diversified qos requirements," in *ICC 2019-2019 IEEE International Conference on Communications (ICC)*, pp. 1–6, IEEE, 2019.

[3] E. A. Jorswieck, "Next-Generation Multiple Access: From Basic Principles to Modern Architectures," *Proceedings of the IEEE*, vol. 112, no. 9, pp. 1149–1178, 2024.

[4] P. Singh and S.-Y. Jung, "Modulation and multiple access for beyond 6g electromagnetic nanonetworks in the terahertz band," *IEEE Access*, vol. 13, pp. 13655–13674, 2025.

[5] C. You, Y. Cai, Y. Liu, M. Di Renzo, T. M. Duman, A. Yener, and A. Lee Swindlehurst, "Next generation advanced transceiver technologies for 6g and beyond," *IEEE Journal on Selected Areas in Communications*, vol. 43, no. 3, pp. 582–627, 2025.

[6] G. Smith, "Choice of fdma/scpc access technique for aeronautical satellite voice system," in *Jet Propulsion Lab., California Inst. of Tech., Proceedings of the Mobile Satellite System Architectures and Multiple Access Techniques Workshop*, 1989.

[7] D. Falconer, F. Adachi, and B. Gudmundson, "Time division multiple access methods for wireless personal communications," *IEEE Communications Magazine*, vol. 33, no. 1, pp. 50–57, 1995.

[8] T. Hwang, C. Yang, G. Wu, S. Li, and G. Y. Li, "OFDM and Its Wireless Applications: A Survey," *IEEE Transactions on Vehicular Technology*, vol. 58, pp. 1673–1694, May 2009.

[9] H. G. Myung, J. Lim, and D. J. Goodman, "Single carrier fdma for uplink wireless transmission," *IEEE Vehicular Technology Magazine*, vol. 1, no. 3, pp. 30–38, 2006.

[10] E. Dahlman, S. Parkvall, and J. Skold, *5G NR: The next generation wireless access technology*. Academic Press, 2020.

[11] S. H. Han and J. H. Lee, "An overview of peak-to-average power ratio reduction techniques for multicarrier transmission," *IEEE Wireless Communications*, vol. 12, no. 2, pp. 56–65, 2005.

[12] S. Sen, R. Senguttuvan, and A. Chatterjee, "Environment-adaptive concurrent companding and bias control for efficient power-amplifier operation," *IEEE Transactions on Circuits and Systems I: Regular Papers*, vol. 58, no. 3, pp. 607–618, 2011.

[13] Y. Rahmatallah and S. Mohan, "Peak-to-average power ratio reduction in ofdm systems: A survey and taxonomy," *IEEE Communications Surveys & Tutorials*, vol. 15, no. 4, pp. 1567–1592, 2013.

[14] N. Ali, R. Almahainy, A. Al-Shabili, N. Almoosa, and R. Abd-Alhameed, "Analysis of improved μ-law companding technique for ofdm systems," *IEEE Transactions on Consumer Electronics*, vol. 63, no. 2, pp. 126–134, 2017.

[15] Y. Chen, J. A. Zhang, and A. D. Jayalath, "Estimation and compensation of clipping noise in ofdma systems," *IEEE Transactions on Wireless Communications*, vol. 9, no. 2, pp. 523–527, 2010.

[16] K. S. Ramtej and S. Anuradha, "New error function companding technique to minimize papr in lte uplink communications," in *2017 Twenty-third National Conference on Communications (NCC)*, pp. 1–5, 2017.

[17] S. Cho and S. K. Park, "A new selected mapping scheme without additional ifft operations in ofdm systems," *IEEE Transactions on Consumer Electronics*, vol. 57, no. 4, pp. 1513–1518, 2011.

[18] A. Jayalath and C. Tellambura, "Slm and pts peak-power reduction of ofdm signals without side information," *IEEE Transactions on Wireless Communications*, vol. 4, no. 5, pp. 2006–2013, 2005.

[19] S.-H. Wang, J.-C. Sie, C.-P. Li, and Y.-F. Chen, "A low-complexity papr reduction scheme for ofdma uplink systems," *IEEE Transactions on Wireless Communications*, vol. 10, no. 4, pp. 1242–1251, 2011.

[20] Y. Hori and H. Ochiai, "A new uplink multiple access based on ofdm with low papr, low latency, and high reliability," *IEEE Transactions on Communications*, vol. 66, no. 5, pp. 1996–2008, 2018.

[21] T. Jiang and X. Li, "Using fountain codes to control the peak-to-average power ratio of ofdm signals," *IEEE Transactions on Vehicular Technology*, vol. 59, no. 8, pp. 3779–3785, 2010.

[22] S. B. Slimane, "Reducing the peak-to-average power ratio of ofdm signals through precoding," *IEEE Transactions on Vehicular Technology*, vol. 56, no. 2, pp. 686–695, 2007.

[23] R. Xu, L. Wang, Z. Geng, H. Deng, L. Peng, and L. Zhang, "A unitary precoder for optimizing spectrum and papr characteristic of ofdma signal," *IEEE Transactions on Broadcasting*, vol. 64, no. 2, pp. 293–306, 2018.

[24] Y. A. Al-Jawhar, K. N. Ramli, A. Mustapha, S. A. Mostafa, N. S. Mohd Shah, and M. A. Taher, "Reducing papr with low complexity for 4g and 5g waveform designs," *IEEE Access*, vol. 7, pp. 97673–97688, 2019.

[25] Y. Huleihel and H. H. Permuter, "Low papr mimo-ofdm design based on convolutional autoencoder," *IEEE Transactions on Communications*, vol. 72, no. 5, pp. 2779–2792, 2024.

[26] Y. Huleihel, E. Ben-Dror, and H. H. Permuter, "Low papr waveform design for ofdm systems based on convolutional autoencoder," in *2020 IEEE International Conference on Advanced Networks and Telecommunications Systems (ANTS)*, pp. 1–6, 2020.

[27] T. Zhang, Z. Tong, W. Zhang, H. Wang, and P. Li, "A novel papr reduction scheme based on joint traditional algorithm and machine learning for co-ofdm systems," *IEEE Photonics Technology Letters*, vol. 35, no. 8, pp. 418–421, 2023.

[28] A. Kumar and A. Nanthaamornphong, "Nn-pts: a neural network-assisted papr reduction technique for otfs with high-order modulation," *High Energy Density Physics*, p. 101225, 2025.

[29] X. Wang, N. Jin, and J. Wei, "A model-driven dl algorithm for papr reduction in ofdm system," *IEEE Communications Letters*, vol. 25, no. 7, pp. 2270–2274, 2021.

[30] M. Kim, W. Lee, and D.-H. Cho, "A novel papr reduction scheme for ofdm system based on deep learning," *IEEE Communications Letters*, vol. 22, no. 3, pp. 510–513, 2018.

[31] I. Cinemre and G. Hacioglu, "A dct/dst based fast ofdm method in im/dd systems," *IEEE Communications Letters*, vol. 25, no. 9, pp. 3013–3016, 2021.

[32] B. Cenikliogˇlu, A. Ozen, and I. Develi, "Zt dwt-s owdm: A new waveform for papr reduction," in *2018 41st International Conference on Telecommunications and Signal Processing (TSP)*, pp. 1–4, 2018.

[33] C. Van Bouwel, J. Potemans, S. Schepers, B. Nauwelaers, and A. Van de Capelle, "Wavelet packet based multicarrier modulation," in *IEEE Benelux chapter on vehicular technology and communications. Symposium on communications and vehicular technology. SCVT-2000. Proceedings (Cat. No. 00EX465)*, pp. 131–138, IEEE, 2000.

[34] C.-L. Wang, C.-H. Chang, J. L. Fan, and J. M. Cioffi, "Discrete hartley transform based multicarrier modulation," in *2000 IEEE International Conference on Acoustics, Speech, and Signal Processing. Proceedings (Cat. No. 00CH37100)*, vol. 5, pp. 2513–2516, IEEE, 2000.

[35] L. de M. B. A. Dib, G. R. Colen, M. de L. Filomeno, and M. V. Ribeiro, "Orthogonal chirp division multiplexing for baseband data communication systems," *IEEE Systems Journal*, vol. 14, no. 2, pp. 2164–2174, 2020.

[36] N. V. Kalpage, P. Priya, and Y. Hong, "Dct-based otfs with reduced papr," *IEEE Communications Letters*, vol. 28, no. 1, pp. 158–162, 2024.

[37] Y. Chen, H. Liu, Z. Lu, and H. Wang, "Block scalable ofdm-based waveform for ntn uplink–a comparative study of multiple candidate waveforms over ntn scenarios using nr numerology," *IEEE Access*, vol. 12, pp. 31262–31278, 2024.

[38] P. P. Vaidyanathan, "Ramanujan sums in the context of signal processing-Part II: FIR representations and applications," *IEEE Trans. Signal Process.*, vol. 62, pp. 4158–4172, Aug. 2014.

[39] P. Saidi, G. Atia, and A. Vosoughi, "On robust detection of brain stimuli with Ramanujan periodicity transforms," in *Proc. 51st Asilomar Conf. Signals, Syst. Comput.*, pp. 729–733, Oct. 2017.

[40] B. Shah Shaik, V. K. Chakka, S. Goli, and A. S. Reddy, "Removal of narrowband interference (PLI in ECG signal) using Ramanujan periodic transform (RPT)," in *Proc. Int. Conf. Signal Process. Commun.*, pp. 233–237, 2016.

[41] P. Saidi, A. Vosoughi, and G. Atia, "Detection of brain stimuli using Ramanujan periodicity transforms," *J. Neural Eng.*, vol. 16, p. 036021, apr 2019.

[42] S. B. Shah, *Signal Representations for Period and Frequency Extraction from a Finite Length Signal*. PhD thesis, Shiv Nadar University, 2021.

[43] S. B. Shah and V. K. Chakka, "Joint reduction of baseline wander, PLI and its harmonics in ECG signal using Ramanujan Periodic Transform," in *2016 IEEE Annual India Conference (INDICON)*, pp. 1–5, Dec 2016.

[44] B. S. Shaik, V. K. Chakka, and S. Goli, "Ramanujan and DFT mixed basis representation for removal of PLI in ECG signal," in *Proc. 4th Int. Conf. Signal Process. Integrated Netw.*, pp. 509–512, Feb 2017.

[45] P. Mathur, V. K. Chakka, and S. B. Shah, "Ramanujan periodic subspace based epileptic eeg signals classification," *IEEE Sensors Lett.*, vol. 5, no. 7, pp. 1–4, 2021.

[46] S. Sural, S. B. Shah, N. T. Ali, and V. K. Chakka, "Different dna encoding schemes for filter bank based tandem repeat detection," in *2025 International Conference on Innovation in Computing and Engineering (ICE)*, pp. 1–5, 2025.

[47] P. P. Vaidyanathan, "Ramanujan sums in the context of signal processing-Part I: Fundamentals," *IEEE Trans. Signal Process.*, vol. 62, pp. 4145–4157, Aug. 2014.

[48] G. Srikanth, V. K. Chakka, and S. B. Shah, "Ramanujan periodic subspace division multiplexing," *IET Commun.*, vol. 13, no. 15, pp. 2296–2303, 2019.

[49] S. B. Shah, N. T. Ali, G. Srikanth, A. Altunaiji, and D. I. Olćan, "Papr performance evaluation of ofdm, rpdm, and orpdm multicarrier modulation schemes," *IEEE Open Journal of the Communications Society*, vol. 6, pp. 5297–5318, 2025.

[50] R. Giuliano, "From 5g-advanced to 6g in 2030: New services, 3gpp advances, and enabling technologies," *IEEE Access*, vol. 12, pp. 63238–63270, 2024.

[51] G. H. Hardy, E. M. Wright, *et al.*, *An introduction to the theory of numbers*. Oxford university press, 1979.

[52] S. Ramanujan, "On certain trigonometrical sums and their applications in the theory of numbers," *Trans. Cambridge Philos. Soc.*, vol. 22, no. 13, pp. 259–276, 1918.

[53] Y. S. Cho, J. Kim, W. Y. Yang, and C. G. Kang, *MIMO-OFDM wireless communications with MATLAB*. John Wiley & Sons, 2010.

[54] S. V. Tenneti and P. P. Vaidyanathan, "Nested Periodic Matrices and Dictionaries: New Signal Representations for Period Estimation," *IEEE Transactions on Signal Processing*, vol. 63, pp. 3736–3750, July 2015.

[55] B. S. Shaik, V. K. Chakka, and A. S. Reddy, "A new signal representation using complex conjugate pair sums," *IEEE Signal Process. Lett.*, vol. 26, pp. 252–256, Feb. 2019.

[56] S. B. Shah, V. K. Chakka, and A. S. Reddy, "On Complex Conjugate Pair Sums and Complex Conjugate Subspaces," *IEEE Signal Process. Lett.*, vol. 26, pp. 1403–1407, Sep. 2019.

[57] S. B. Shah, V. K. Chakka, A. S. Reddy, G. Srikanth, N. T. Ali, A. Altunaiji, M. Alhajri, D. Olcan, and R. Abd-Alhameed, "Properties of type-2 complex conjugate pair sums and their applications," *APSIPA Transactions on Signal and Information Processing*, vol. 13, no. 1, pp. –, 2024.

[58] S. B. Shah, V. K. Chakka, and A. S. Reddy, "Orthogonal and Non-Orthogonal Signal Representations Using New Transformation Matrices Having NPM Structure," *IEEE Trans. Signal Process.*, vol. 68, pp. 1229–1242, 2020.

[59] W. Hoeffding, "Probability inequalities for sums of bounded random variables," *Journal of the American Statistical Association*, vol. 58, no. 301, pp. 13–30, 1963.

[60] S. S. Sefati, A. U. Haq, Nidhi, R. Craciunescu, S. Halunga, A. Mihovska, and O. Fratu, "A comprehensive survey on resource management in 6g network based on internet of things," *IEEE Access*, vol. 12, pp. 113741–113784, 2024.

[61] S.-C. Pei and K.-W. Chang, "Closed-form orthogonal ramanujan integer basis," *IEEE Signal Processing Letters*, vol. 24, no. 1, pp. 116–120, 2017.

[62] C.-Y. Chao, "Circulant matrices (philip j. davis)," *SIAM Review*, vol. 24, no. 3, p. 356, 1982.